A cytochrome c is the natural electron acceptor for nicotine oxidoreductase

Mark Dulchavsky[1,2], **Christopher T. Clark**[3], **James C. A. Bardwell**[1,4,*], **Frederick Stull**[3,*]

[1]Howard Hughes Medical Institute, University of Michigan, Ann Arbor, MI, USA.

[2]Cellular and Molecular Biology Program, University of Michigan, Ann Arbor, MI, USA.

[3]Department of Chemistry, Western Michigan University, Kalamazoo, MI, USA.

[4]Department of Molecular, Cellular and Developmental Biology, University of Michigan, Ann Arbor, MI, USA.

Abstract

Nicotine oxidoreductase (NicA2), a member of the flavin-containing amine oxidase family, is of medical relevance as it shows potential as a therapeutic to aid cessation of smoking due to its ability to oxidize nicotine into a non-psychoactive metabolite. However, the use of NicA2 in this capacity is stymied by its dismal O_2-dependent activity. Unlike other enzymes in the amine oxidase family, NicA2 reacts very slowly with O_2, severely limiting its nicotine-degrading activity. Instead of using O_2 as an oxidant, we discovered that NicA2 donates electrons to a cytochrome c, which means that NicA2 is actually a dehydrogenase. This is surprising, as enzymes of the flavin-containing amine oxidase family were invariably thought to use O_2 as an electron acceptor. Our findings establish new perspectives for engineering this potentially useful therapeutic and prompt a reconsideration of the term "oxidase" in referring to members of the flavin-containing amine "oxidase" family.

Introduction

Flavin-dependent enzymes most often utilize their flavin adenine dinucleotide (FAD) or flavin mononucleotide cofactors to conduct reduction-oxidation chemistry. These enzymes are able to pass electrons between their cofactor and substrate in one or two-electron transfer reactions[1]. Some flavoenzymes, termed oxidases, rapidly deliver electrons to molecular oxygen (O_2), creating reactive oxygen species such as superoxide or hydrogen peroxide as a

byproduct. Other flavoenzymes are more discerning, instead donating electrons to specific proteins or small molecule substrates. These enzymes are defined as dehydrogenases and generally do not react rapidly with O_2. However, some degree of oxygen reactivity is inevitable in most flavin-dependent enzymes that form the flavin hydroquinone state due to the ~1 V reduction potential difference between flavins and O_2. Flavin-containing amine oxidases (pfam:01593)[2] are rapidly re-oxidized by O_2 after accepting electrons from their amine-containing substrates. This rapid re-oxidation is evident, at least *in vitro*, for nearly all previously characterized members of this enzyme family[3–5]. Nicotine oxidoreductase (NicA2), however, appears to defy this convention, reacting with oxygen very slowly.

NicA2 is a FAD-dependent enzyme that catalyzes the oxidation of nicotine into N-methylmyosmine[6]. It was isolated from *Pseudomonas putida* S16, an unusual microorganism that can achieve robust growth using nicotine as its sole carbon and nitrogen source[7]. NicA2 catalyzes the first step in the catabolic pathway, which eventually results in the production of fumarate for primary metabolism[8]. NicA2's FAD cofactor accepts a hydride from nicotine, converting it into N-methylmyosmine in the enzyme's biologically important reductive half-reaction[9]. N-methylmyosmine then undergoes spontaneous hydrolysis to pseudooxynicotine, which is non-toxic and non-addictive in animal models[10]. Because of this, NicA2 has recently received attention as a potential therapeutic for treating nicotine dependence[10–13]. Two recent studies revealed that injection of NicA2 into nicotine-dependent rats largely eliminated nicotine from the blood, reversed symptoms of nicotine withdrawal, and dramatically reduced compulsive nicotine consumption and susceptibility to relapse[11,13].

NicA2 receives two electrons from nicotine. In order to function as a catalyst, the two electrons retained on NicA2's FAD from nicotine oxidation must be transferred to an electron acceptor. Given NicA2's homology to flavin-dependent amine oxidases that transfer their electrons directly to O_2, studies to date have assumed that O_2 directly accepts the electrons from NicA2's reduced FAD[9,12]. However, NicA2 has a turnover number of 0.007 s^{-1} when using O_2 as a terminal electron acceptor[10,14,15], an abysmally low number when compared with other flavin-containing amine oxidases which have turnover numbers of ~10–100 s^{-1} [16–18]. NicA2's poor activity as an oxidase is an obstacle in developing this enzyme for nicotine cessation therapy. The low catalytic activity of the enzyme requires prohibitively large doses of NicA2, up to 70 mg kg^{-1}, to achieve symptomatic relief of nicotine-dependent behavior in rats[11]. A previous study suggested that NicA2 may use a more effective electron acceptor, but did not propose any specific candidates[14].

Here, we demonstrate that a novel cytochrome c protein, dubbed CycN, is responsible for accepting electrons from reduced NicA2 *in vivo*, not O_2. Our results open up new avenues for using NicA2 in treating nicotine dependence and suggest that other flavin-dependent amine oxidases may also use alternative physiologic electron acceptors.

Results

NicA2 reacts poorly with O_2.

The flavin cofactor contained in the nicotine-degrading enzyme NicA2 provides a convenient spectrophotometric readout for NicA2's oxidation status[1]. In the absence of

nicotine, NicA2 has an absorbance spectrum typical for oxidized FAD (Fig. 1a). Upon the addition of nicotine to NicA2, however, a clear reduction of FAD to the two-electron reduced hydroquinone ($FADH_2$) was seen. NicA2's flavin remained in the $FADH_2$ state for several minutes before slowly re-oxidizing directly to oxidized FAD. This slow re-oxidation of NicA2 in the presence of oxygen suggests that flavin re-oxidation may be rate-limiting during O_2-dependent turnover.

Like most flavin-dependent enzymes, the catalytic cycle of NicA2 can be divided into two half-reactions. In the reductive half-reaction, NicA2 containing oxidized FAD (NicA2-Fl_{ox}) is reduced by reacting with nicotine to form N-methylmyosmine. In the oxidative half-reaction, NicA2 containing $FADH_2$ (NicA2-Fl_{red}) is oxidized by reacting with O_2. To quantitatively determine the extent to which NicA2-Fl_{red} oxidation by O_2 limits the consumption of nicotine by NicA2, we examined each half-reaction separately by performing stopped-flow experiments. Reduction of anaerobic NicA2-Fl_{ox} by nicotine in the reductive half-reaction was extremely rapid (Fig. 1b). The observed rate constant (k_{obs}) for each of the three phases observed did not change with increasing nicotine concentrations (Fig. 1b inset), suggesting that all three events occur after the bimolecular step in which nicotine first binds to NicA2-Fl_{ox}. The first two phases (k_{obs} of ~620 s^{-1} and ~130 s^{-1}) contribute 95% of the signal change at 450 nm and have approximately the same amplitudes; the UV-vis spectra observed at the end of these two phases suggest that both correspond to FAD reduction by nicotine (Extended Data Fig. 1a). That there are two phases may indicate that the two active sites of the NicA2 dimer may be reduced by nicotine with discrete rate constants (Extended Data Fig. 2). The change in UV-vis spectrum for the final phase (k_{obs} of ~6.6 s^{-1}) is consistent with a ligand exchange event following FAD reduction by nicotine. This phase may represent exchange of N-methylmyosmine product with the available excess nicotine. Traces at all nicotine concentrations extrapolated back to the absorbance of NicA2-Fl_{ox} at time zero (Extended Data Fig. 1b). Notably, the reductive half-reaction is completed within 1 s. That k_{obs} for all three phases did not increase as the nicotine concentration was raised indicates that nicotine concentrations used were saturating and suggests that nicotine binds rapidly prior to FAD reduction. To further assess the possibility of rapid substrate binding, we measured binding kinetics using the non-catalytic nicotine analog myosmine. Myosmine binding was completed within the 1 ms dead time of the instrument at all myosmine concentrations (Extended Data Fig. 3), indicating that myosmine binds to NicA2-Fl_{ox} with a k_{obs} substantially greater than the rate constant for FAD reduction by nicotine.

We next monitored the reaction of NicA2-Fl_{red} with O_2 in the oxidative half-reaction. NicA2-Fl_{red} was prepared by titrating NicA2-Fl_{ox} with one equivalent of dithionite. The use of dithionite as a reductant enabled us to study the oxidative half-reaction in the absence of nicotine reaction products. During the dithionite titration, NicA2's FAD first populated a form with a UV-vis spectrum resembling a neutral flavin semiquinone[19] before reaching the fully reduced $FADH_2$ state (Extended Data Fig. 1c). This suggests that NicA2 is capable of stabilizing a one-electron reduced flavin. Once fully reduced, NicA2-Fl_{red} was then mixed with buffer equilibrated with various O_2/N_2 ratios to re-oxidize NicA2's flavin. Flavin re-oxidation by O_2 was dramatically slower than the reductive half-reaction with nicotine, taking ~400 s for re-oxidation at 540 μM O_2 (Extended Data Fig. 4a). NicA2-Fl_{red} oxidized directly into NicA2-Fl_{ox} (Fig. 1c). Kinetic traces at 450 nm could be fit with a single

exponential and the k_{obs} for this phase increased linearly with O_2 concentration (Fig. 1c inset and 1d), indicating that O_2 directly oxidizes NicA2-Fl$_{red}$ into NicA2-Fl$_{ox}$ in a bimolecular reaction. Linear fitting of k_{obs} against $[O_2]$ yielded a bimolecular rate constant for flavin oxidation (k_{ox}^{O2}) of 27 ± 1 $M^{-1}s^{-1}$. We also measured k_{ox}^{O2} for NicA2 reduced with one equivalent of nicotine instead of dithionite to test if the presence of the N-methylmyosmine product affects NicA2-Fl$_{red}$ oxidation by O_2. Titrating NicA2-Fl$_{ox}$ with one equivalent of nicotine produced a charge-transfer band from 500–700 nm as the FAD was reduced, indicating that the N-methylmyosmine product stays bound to NicA2-Fl$_{red}$ after reduction (Extended Data Fig. 1d). N-methylmyosmine-bound NicA2-Fl$_{red}$ was oxidized even slower by O_2 than NicA2-Fl$_{red}$ in the absence of N-methylmyosmine (Extended Data Fig. 4b,4c), with a k_{ox}^{O2} value of 5 ± 1 $M^{-1}s^{-1}$ (Extended Data Fig. 4d). Our data indicate that O_2 is a poor electron acceptor for NicA2-Fl$_{red}$, particularly when compared to the k_{ox}^{O2} values of 10^5–10^6 $M^{-1}s^{-1}$ seen for most flavin-containing amine oxidases[20].

Identification of NicA2's physiological electron acceptor.

P. putida S16 is able to grow with a doubling time of about 90 min using nicotine as its sole carbon and nitrogen source[7]. At the established *in vitro* catalytic rate of NicA2 using O_2[10], it is impossible to accumulate enough biomass from nicotine to sustain this doubling time. Even if 5% of *P. putida* S16's biomass was made up of NicA2 enzyme, we calculate that this enzyme must have a catalytic rate of at least 1 s^{-1} *in vivo* to support a 90 min doubling time (see Online Methods). This implies that NicA2 uses a different electron acceptor *in vivo*.

The genome of *P. putida* S16 indicates a poorly annotated open reading frame (PPS_RS28240) just downstream of *nicA2* (Fig. 2a)[6,7,21]. Both *nicA2* and this open reading frame possess signal sequences for periplasmic localization (SignalP 5.0[22]). A BLAST search of the downstream open reading frame revealed homology to cytochrome c proteins (Extended Data Fig. 5), and we therefore designate this gene as *cycN*. Cytochromes c are small electron carrier proteins that mediate electron transfer reactions, such as those between complex III and complex IV of the aerobic electron transport chain[23]. This, and the fact that *cycN* forms an operon with *nicA2* led us to hypothesize that CycN plays a similar role for NicA2, shuttling electrons between NicA2 and the electron transport chain.

P. putida S16 *cycN* is unable to grow on nicotine.

To test if CycN is NicA2's physiological electron acceptor, an in-frame deletion of *cycN* was assessed for its ability to grow on nicotine[24]. Both the *cycN* and wild-type (WT) strains grew well on rich media. When plated onto media where nicotine is the sole carbon and nitrogen source, the *cycN* strain showed a growth defect (Fig. 2b). While WT *P. putida* S16 formed large, easily visible colonies within two days, the *cycN* strain grew poorly. Presumably this is because in the absence of CycN, NicA2 is forced to use other electron acceptors such as O_2, causing poor growth. The nicotine growth phenotype of the *cycN* strain was complemented by plasmid-based expression of *cycN* (Fig. 2b), confirming that the growth deficiency is due to the loss of *cycN*. *In vivo* nicotine consumption experiments demonstrate that *cycN* is also necessary for NicA2's ability to degrade nicotine (Fig. 2c,d). The NicA2 protein level is similar in WT and *cycN* strains; however, while the WT strain

consumed all the nicotine in the culture, the *cycN* strain showed minimal nicotine consumption. This indicates that NicA2's activity is dramatically reduced in the absence of CycN, in agreement with CycN being NicA2's physiological electron acceptor. That nicotine is not degraded in *cycN* strains makes it unlikely that any alternative oxidants make a physiologically important contribution toward re-oxidation of NicA2 *in vivo*.

CycN is reduced by NicA2.

Flavin-dependent dehydrogenases are known to transfer their electrons to a variety of small molecules and protein clients, including cytochromes c[25,26]. To further probe the relationship between NicA2 and CycN, we recombinantly expressed and purified both proteins from *Escherichia coli* to characterize their *in vitro* electron transfer activities. We used the spectral differences in the redox status for heme in cytochrome c[27] as a readout to determine if NicA2 can transfer electrons from nicotine to CycN. Upon incubation of oxidized CycN with excess nicotine and a catalytic amount of NicA2, a characteristic shift of the Soret-banding pattern occurred, indicating that CycN had become reduced (Fig. 3). This reduction in CycN required both nicotine and NicA2. NicA2 also produces H_2O_2 when aerobically degrading nicotine in the absence of CycN, but not when CycN is provided (Extended Data Fig. 6a).

NicA2-Fl$_{red}$ is rapidly re-oxidized by CycN.

To measure the rate at which electrons are transferred from NicA2-Fl$_{red}$ to oxidized CycN (CycN$_{ox}$) *in vitro*, we performed stopped-flow absorbance experiments by anaerobically mixing 15 μM NicA2-Fl$_{red}$ with an excess of CycN$_{ox}$. Electron transfer between NicA2-Fl$_{red}$ and CycN$_{ox}$ was complete in less than 1 second. The absorbance changes were dominated by signals associated with reduction of CycN$_{ox}$'s heme from the Fe^{3+} to the Fe^{2+} state (CycN$_{red}$) (Fig. 4a). We analyzed the kinetics of the reaction at 542 nm because the absorbance of CycN$_{ox}$ and CycN$_{red}$ is identical at 542 nm so this readout is unaffected by changes in CycN's oxidation state (Extended Data Fig. 7), and because NicA2's flavin semiquinone (NicA2-Fl$_{SQ}$) absorbs at this wavelength, unlike NicA2-Fl$_{ox}$ and NicA2-Fl$_{red}$ (Extended Data Fig. 1c). This wavelength therefore allowed us to monitor the expected transient formation of NicA2-Fl$_{SQ}$, since CycN$_{ox}$ is an obligate one-electron acceptor and two CycN$_{ox}$ molecules must react sequentially with NicA2-Fl$_{red}$ in order to fully oxidize it back into NicA2-Fl$_{ox}$. Kinetic traces of the reaction with more than a two-fold molar excess of CycN$_{ox}$ indeed showed an increase, followed by a decrease in absorbance at 542 nm (Fig. 4a inset), in agreement with the formation of NicA2-Fl$_{SQ}$ followed by its conversion to NicA2-Fl$_{ox}$. We further tested that the signal changes at 542 nm report on NicA2-Fl$_{SQ}$ by mixing NicA2-Fl$_{red}$ with an equimolar amount of CycN$_{ox}$. Here we should only observe the increase at 542 nm, as there is only enough CycN$_{ox}$ to react once on average with NicA2-Fl$_{red}$ given that the first phase is substantially faster than the second. Reaction of 15 μM NicA2-Fl$_{red}$ with 15 μM CycN$_{ox}$ showed only an increase in absorbance at 542 nm without any subsequent decrease, confirming that we are observing formation of the NicA2-Fl$_{SQ}$ at this wavelength (Extended Data Fig. 6b).

Stopped-flow traces at 542 nm using an excess of CycN$_{ox}$ could be fit using a double exponential function. The k_{obs} values for both phases increased linearly with the CycN$_{ox}$

concentration, indicating that they both report on the bimolecular association of NicA2 with $CycN_{ox}$ (NicA2-Fl_{red} and NicA2-Fl_{SQ} in the first and second phase, respectively). Linear fitting of the k_{obs} plots yielded bimolecular rate constants (k_{on}) of $1.0 \pm 0.2 \times 10^6$ $M^{-1}s^{-1}$ and $2.7 \pm 0.2 \times 10^5$ $M^{-1}s^{-1}$ for the first and second phase, respectively (Fig. 4b). Strikingly, these values are ~4–5 orders of magnitude greater than that for the oxidation of NicA2-Fl_{red} by O_2 (which is 27 ± 1 $M^{-1}s^{-1}$). The fact that both phases are bimolecular indicates that electron transfer between $CycN_{ox}$ and NicA2-$Fl_{red/SQ}$ is rate-limited by association between the two proteins. Electron transfer between the two redox centers must therefore be extremely rapid after the complex has formed, and $CycN_{red}$ produced by the first electron transfer must dissociate from NicA2-Fl_{SQ} faster than the second $CycN_{ox}$ binds (Extended Data Fig. 8). CycN does not form a stable complex with NicA2, in agreement with a large dissociation rate constant for the interaction (Extended Data Fig. 6c). Reaction traces at 552 nm, where the signal for $CycN_{red}$ formation dominates, also fit to two phases with k_{obs} values similar to those obtained using the 542 nm data (Extended Data Fig. 9b), confirming that reduction of two $CycN_{ox}$ molecules accompanies the two one-electron oxidations of NicA2's flavin in the reaction.

We also monitored the kinetics of electron transfer between nicotine-reduced NicA2 and $CycN_{ox}$ to see if the presence of the product, N-methylmyosmine, impacts electron transfer between the two proteins. Reaction traces again showed two kinetic phases, consistent with two stepwise one-electron transfers to two $CycN_{ox}$ molecules required to fully oxidize N-methylmyosmine bound NicA2-Fl_{red} (Extended Data Fig. 9c,d). The k_{obs} for both phases increased linearly with $CycN_{ox}$ concentration, indicating that each phase still reports on the two different bimolecular association steps. Linear fitting of the two data sets yielded bimolecular rate constants of $1.4 \pm 0.1 \times 10^5$ $M^{-1}s^{-1}$ and $7.7 \pm 0.3 \times 10^4$ $M^{-1}s^{-1}$ for the first and second phase, respectively (Fig. 4c). Importantly, both of these values are more than 10,000-fold larger than the $k_{ox}{}^{O2}$ of 5 $M^{-1}s^{-1}$ for oxidation of N-methylmyosmine-bound NicA2-Fl_{red} by O_2, indicating that CycN is a much more effective oxidant for NicA2-Fl_{red} than O_2 when N-methylmyosmine is bound.

Electron transfer to CycN limits turnover by NicA2.

We next used steady-state kinetic experiments of the NicA2-catalyzed electron transfer from nicotine to CycN to identify the rate-determining kinetic event. The reaction rate using saturating concentrations of nicotine increased linearly with CycN concentration over the accessible range of CycN concentrations (5–128 μM CycN). Presumably the reaction rate would saturate at higher CycN concentrations. Converting the rate data to apparent turnover numbers revealed that the apparent turnover number data was nearly identical to that of the second $CycN_{ox}$ binding event for N-methylmyosmine-bound NicA2-Fl_{red} (Fig. 4d). This observation suggests that N-methylmyosmine remains bound to NicA2-Fl_{red} during electron transfer to $CycN_{ox}$ and that binding of $CycN_{ox}$ to NicA2-Fl_{SQ} is rate-determining at CycN concentrations 128 μM. This also suggests that the third phase in the reductive half-reaction with nicotine is not catalytically relevant since our measured apparent turnover numbers are larger than the k_{obs} of ~6.6 s^{-1} for that step.

NicA2-Fl$_{red}$ reacts poorly with bovine cytochrome c.

Is reactivity with NicA2 specific to CycN or will any cytochrome c work? Bovine cytochrome c (43% sequence identity to CycN), which is commonly used in the study of the electron transport chain, was tested as an electron acceptor for NicA2. It was not efficiently reduced, suggesting that NicA2 is specific for CycN (Extended Data Fig. 10a). Structural models of CycN indicate that the surface of bovine cytochrome c is enriched in positive charge relative to CycN, especially in the region near exposed heme (Extended Data Fig. 10b). Positively charged lysine residues are important for bovine cytochrome c binding to cytochrome oxidase[28], so this difference in charge distribution between CycN and bovine cytochrome c may be partially responsible for NicA2's specificity for CycN.

Discussion

We have demonstrated that a novel cytochrome c, CycN, is the physiological oxidant for NicA2, not O$_2$. NicA2 is therefore a dehydrogenase, making it a notable outlier within the flavin-containing amine oxidase superfamily. We found that biphasic hydride transfer between nicotine and NicA2-Fl$_{ox}$ in the reductive half-reaction occurs rapidly. This is followed by a slower kinetic event that may correspond to dissociation of N-methylmyosmine. However, this slow step is unlikely to be relevant during turnover since our data suggest that N-methylmyosmine remains bound when NicA2 reacts with CycN. Re-oxidation of NicA2-Fl$_{red}$ by CycN must occur in a sequence of two one-electron transfer reactions since each molecule of CycN can only receive one electron. Based on our data, both of these one-electron transfers appear to be rate-limited by the interaction between NicA2 and CycN; the subsequent electron transfer must be substantially faster than binding. These points are summarized in Figure 5. Oxidation of NicA2-Fl$_{red}$ by O$_2$ is unlikely to contribute substantially to nicotine turnover *in vivo* since O$_2$ oxidizes NicA2-Fl$_{red}$ with a rate constant ~10,000–15,000 times lower than its oxidation by CycN.

Our discovery that NicA2 is a dehydrogenase that uses CycN as an electron acceptor raises many interesting questions about how NicA2 discriminates between CycN and O$_2$. NicA2 appears to be specific for CycN since bovine cytochrome c is a poor recipient of electrons from NicA2, suggesting that CycN contains structural features that optimize its reactivity or are important for binding to NicA2. Structures show that the isoalloxazine of NicA2's FAD is buried within the protein core, >10 Å away from the surface. Can one-electron transfers between NicA2's isoalloxazine and CycN's heme span this distance, or are major conformational changes or protein-derived wires required for electron transfer between these redox centers? NicA2's poor reactivity with O$_2$ is also difficult to rationalize based on structures, as NicA2's FAD binding site is very similar to that in a homologous protein that reacts rapidly with O$_2$, namely 6-hydroxy-L-nicotine oxidase (Supplementary Fig. 1)[29,30]. Two recent studies attempted to screen NicA2 variants with residue mutations near the isoalloxazine or the presumed product exit site for improved O$_2$-dependent nicotine-degrading activity[12,31]. However, NicA2 variants with only modest improvements were identified, suggesting that O$_2$ reactivity in NicA2 is not controlled by structural features near the isoalloxazine. How reactivity with O$_2$ is suppressed in NicA2 is thus currently unclear.

Microorganisms sometimes find ways to obtain energy and nutrients from surprising sources. For *P. putida* S16, CycN provides an illustration of one such adaptation. Rather than transferring electrons from nicotine directly to O_2, which would waste valuable reducing equivalents and create H_2O_2, electrons are shuttled from NicA2 to CycN. Cytochrome c proteins are not known to be terminal electron acceptors. Thus, the electrons obtained by CycN from nicotine oxidation must be passed to another electron acceptor to enable continued turnover by NicA2. Where these electrons are transferred, and their eventual fate, is unknown. Other *Pseudomonas* subspecies conduct aerobic respiration using cytochrome c oxidases such as the cbb3 cytochrome oxidase of *Pseudomonas aeruginosa*[32,33]. Since *P. putida* S16 seems to contain similar machinery (Supplementary Fig. 2), this may provide an avenue for CycN re-oxidation. Regardless of the pathway that electrons take from CycN, CycN is clearly required for robust growth of the organism on nicotine.

Several recent studies have demonstrated NicA2's potential utility as treatment for nicotine dependence[10,11]. One important caveat to these studies is the prohibitively large protein amounts required to achieve effective treatment—at least 10 and up to 70 mg kg^{-1} daily[11], considerably more than is feasible for humans. Accordingly, there is interest in generating NicA2 variants with increased nicotine turnover rates. One avenue for enhancing therapeutic nicotine turnover suggested by our work is to co-administer CycN alongside NicA2. Another option would be to engineer NicA2 to enhance its oxidase activity. This may be possible given that NicA2 belongs to a family where most members react rapidly with O_2. Site-saturation mutagenesis of NicA2's active site[12] enabled the identification of several mutations that allowed for an up to 19-fold increased turnover rate of nicotine with O_2. These are relatively modest increases, given that NicA2 can re-oxidize at >10,000 times the rate of re-oxidation with O_2 when provided its physiologic electron acceptor, implying that activity with O_2 could perhaps be further improved.

Applying the lessons learned from NicA2 more generally, members of the flavin-dependent amine oxidase family are assumed to undergo oxidation by O_2 *in vivo* and typically readily re-oxidize with O_2 *in vitro*[4]. That NicA2 transfers electrons to a c-type cytochrome prompts reconsideration of this generalization and raises the possibility that other members of this family use alternative physiological oxidants. When amine oxidases use O_2 as an oxidant, reactive oxygen species such as H_2O_2 are released as a byproduct[34]. It may therefore be more desirable to shunt electrons elsewhere *in vivo*, as we have shown occurs with NicA2 in *P. putida* S16. Furthermore, just because an amine oxidase is able to be rapidly oxidized by O_2 *in vitro* does not necessarily mean that it uses O_2 as its preferred electron acceptor *in vivo*. There is circumstantial evidence for the existence of one such example in human monoamine oxidases (MAOs) A and B[35]. These enzymes are bound to the outer mitochondrial membrane by a transmembrane tail anchor[36–38]. In their presumed catalytic cycle, MAOs are thought to be re-oxidized by O_2, producing potentially damaging H_2O_2[39]. Recent work, however, has demonstrated that human MAOs are not creating H_2O_2 as previously thought, and instead seem to transfer electrons from amine oxidation to complex IV of the electron transport chain[35]. Given that cytochrome c exists in the mitochondrial intermembrane space, we propose that cytochrome c may be the link facilitating electron transfer to the electron transport chain from MAOs. A re-evaluation of the mechanistic paradigm of these enzymes is indicated. MAOs are frequent targets for *in vitro* drug studies,

and it may be that they are deprived of vital redox cofactors in these studies. Given the role of MAOs in neuropsychiatric disease, this topic warrants further consideration.

In summary, we have demonstrated that NicA2 is a flavin-dependent dehydrogenase that uses CycN as its redox partner. In the continued study of flavoenzymes, the "oxidase" paradigm for flavin-dependent amine oxidases should be reconsidered, as structural similarity alone clearly cannot determine oxygen reactivity.

Methods

Strains and culture conditions.

P. putida S16 was obtained from American Type Culture Collection (ATCC® BAA-2545™). Culture was performed in lysogeny broth (LB) media unless otherwise specified. M9 salts with nicotine media was made with the following: 6 g L^{-1} Na_2HPO_4, 3 g L^{-1} KH_2PO_4, 1 mM $MgSO_4$, 0.1 mM $CaCl_2$, 1 μg mL^{-1}; thiamine, 1 g L^{-1} nicotine. M9 salts with nicotine agar was made with the same recipe, with an additional 15 g L^{-1} bacto agar (Thermo Fisher Scientific). All liquid cultures were inoculated from single colonies streaked out onto selective media. *E. coli* BL21 (DE3) cells were used for protein expression. Protein expression media (PEM) contains 12 g L^{-1} tryptone, 24 g L^{-1} yeast extract, 50.4 g L^{-1} glycerol, 2.13 g L^{-1} K_2HPO_4, and 12.54 g L^{-1} KH_2PO_4.

Construction of vectors.

Standard cloning techniques were used. pEC86 helper vector was obtained from the Culture Collection of Switzerland. pJN105 vector was obtained as a gift from Ute Römling (Karolinska Institute). Genes codon optimized for expression in *E. coli* were purchased from Genscript for *cycN* and *nicA2* and cloned via restriction digest into pET28a, pJN105, or pET22b vectors. The *nicA2* gene, including its N-terminal signal sequence, was cloned into pET28a containing an N-terminal His-SUMO tag. For the complementation experiments, full-length *cycN*, including its native signal sequence, was cloned into pJN105. For protein expression and purification, the sequence for mature *cycN* lacking its signal sequence was cloned downstream of the *pelB* leader sequence in pET22b.

Estimating NicA2 turnover rate *in vivo*.

When grown on nicotine as its sole carbon and nitrogen source, *P. putida* S16 obtains nearly all of its biomass from this metabolite. Using the known values for doubling time, bacterial mass, and the amount of nicotine that must be turned over to sustain growth, we can estimate the minimal nicotine turnover rate for NicA2. A single bacterium's carbon and nitrogen content has a mass of ~0.3 pg, *P. putida* S16 doubles in roughly 90 min when grown on nicotine[7], and nicotine has a molecular weight of 162 g mol^{-1}. Therefore, each bacterium must turn over 2×10^{-15} mol of nicotine to double its mass. Assuming that NicA2 accounts for no more than 5% of total cell mass, there can be no more than 2.8×10^{-19} mol of NicA2 expressed for a single cell. We thus estimate the NicA2 *in vivo* turnover rate as 2×10^{-15} mol nicotine degraded by 2.8×10^{-19} mol NicA2 in 90 min, resulting in a turnover rate of ~1.3 s^{-1}.

NicA2 expression and purification.

The pET28a-based expression vector for NicA2 was transformed into *E. coli* BL21 (DE3) cells and grown in 4 L PEM at 37 °C with shaking to an OD600 of 1.0. The temperature was then lowered to 20 °C and expression induced with 100 μM IPTG. The culture was grown overnight at 20 °C. After harvesting, the cells were lysed at 4 °C by sonication in 50 mM Tris HCl, 400 mM NaCl, 15 mM imidazole, 10% glycerol, pH 8.0 (lysis buffer) with DNase I and cOmplete™ protease inhibitor cocktail. The lysate was cleared by centrifugation and the supernatant was loaded on three 5 mL HisTrap columns pre-equilibrated in lysis buffer. The columns were washed with 20 mL lysis buffer, then 20 mL lysis buffer + 20 mM imidazole, and NicA2 was then eluted in lysis buffer + 0.5 M imidazole. NicA2 was then exchanged into 40 mM Tris-HCl, pH 8 + 0.2 M NaCl in the presence of protease ULP1 to cleave off the His-SUMO tag and subsequently passed over the HisTrap column again in 25 mM Tris HCl, pH 8 + 0.2 M NaCl to remove the His-SUMO tag. Protein was then exchanged into 25 mM Tris pH 8.5 and loaded onto three 5 mL HiTrap Q columns equilibrated into the same buffer. NicA2 was eluted by linear salt gradient using 25 mM Tris pH 8.5 + 1 M NaCl. Fractions containing NicA2 were concentrated, then run over a HiLoad Superdex 200 column in 40 mM HEPES 100 mM NaCl pH 7.4. Purified protein was concentrated and flash frozen, then stored at −80 °C until use (Supplementary Figure 3a).

CycN expression and purification.

The methods in enzymology subsection describing expression and purification of cytochromes c was followed[40]. Antibiotic selection was maintained with chloramphenicol 17 μg mL^{-1} and ampicillin 100 μg mL^{-1} throughout. All incubations were performed at 30 °C. *E. coli* BL21 (DE3) cells were transformed with both pEC86 helper vector and pET22b-*cycN* for periplasmic expression. A single colony of the resulting transformation was inoculated into overnight culture, then subcultured into 3L PEM and incubated at 200 rpm. Cultures were grown to a density of OD 0.6–0.8, then induced with 10 μM IPTG. Cells were left to express overnight for 18–22 h. Red pellets were visible after spinning down at 4,000*g* for 20 min.

Pellets were immediately resuspended for periplasmic extraction by osmotic shock in ice-cold osmotic shock buffer (0.5 M sucrose, 0.2 M Tris HCl, pH 8.0, and 0.5 mM EDTA), 50 mL buffer per L of culture. 33 mL ice-cold water was added after resuspension, and the resulting mixture was incubated on ice with gentle shaking for 2 h. Suspensions were spun down at 12,000 *g* for 20 min, and the red supernatant saved. These supernatants were dialyzed against 4 L of pH 4.0 30 mM sodium citrate + 38 mM Na$_2$HPO$_4$ overnight, then dialyzed into an additional 4 L of 25 mM NaH$_2$PO$_4$ at pH 4.0. The next day, samples were loaded onto a HiTrap SP HP cation exchange column (GE Life Sciences) equilibrated in the same buffer, and eluted against 25 mM NaH$_2$PO$_4$, pH 4.0 + 1 M NaCl in a salt gradient. Final cleanup was performed by running over a HiLoad Superdex 75 size exclusion column equilibrated in 40 mM HEPES 100 mM NaCl pH 7.4. Purified protein was flash frozen and stored at −80 °C until use (Supplementary Figure 3b).

Generation of *cycN* knockout.

A *cycN* knockout was generated by two-step allelic exchange according to the protocol established by Hmelo et al.[24]. Briefly, PCR of *P. putida* S16 genomic DNA was used to amplify regions upstream and downstream of *cycN* using the listed primers (Supplementary Table 1). CycN_del_down primers created a DNA fragment containing the stop codon, the last few amino acids for CycN, and ~500 bp of downstream sequence. CycN_del_up primers created a fragment with ~500 bp of upstream sequence, including the start codon and first few amino acids for CycN. An additional PCR reaction using the set of both products and the primers CycN_del_up_Fwd and CycN_del_down_Rev was used to assemble the fragments together, creating a substrate for homologous recombination against the *P. putida* S16 genome. This was cloned into pEX18-Gm vector by restriction digest. Upon recombining, the *P. putida* S16 homologous fragment will insert next to the *cycN* gene along with the pEX18-Gm sequence containing a gentamycin marker and *sacB* marker for sucrose counterselection. pEX18-Gm cannot replicate in *P. putida* S16, and gentamycin resistance can only be passed on in this strain by genomic integration. Therefore, by first selecting for gentamycin resistance, we generate clones with the integrated genomic marker. Then, counterselecting by plating onto sucrose afterward, we select for clones that undergo a secondary recombination event, removing remaining pEX18-Gm sequence with *sacB* and the majority of *cycN* coding sequence, resulting in a scarless knockout.

pEX18-Gm was electroporated into the mating strain *E. coli* S17. Both *E. coli* S17 and *P. putida* S16 strains were grown at 30 °C until an OD of 1.0 was reached, at which point 5 mL of culture was spun down and resuspended in 1 mL LB. An equal mixture of each strain, 200 μL each, was then spotted onto an LB agar plate for mating overnight at 30 °C. The next day, the spot was scraped and washed three times with 1 mL 150 mM NaCl. The resulting washed cells were resuspended in 500 μL 150 mM NaCl, and serial dilutions were plated on M9 salts + 0.4% glucose + 25 μg mL^{-1} gentamycin plates for selection of *Pseudomonas* with genomic integration of antibiotic marker. This resulted in >100 colonies, 8 of which were re-streaked onto 20% sucrose no-salt LB agar for secondary selection. This resulted in many single colonies, 16 of which were chosen for colony PCR screening using the listed CycN_verify primers, identifying which colonies successfully recombined *cycN* out. Three colonies appeared positive by size of PCR band; these were then gel extracted and submitted for Sanger sequencing, confirming the location and fidelity of knockouts.

Phenotyping wild-type, knockout, and complemented *P. putida* S16.

Single colonies of each strain grown from LB agar plates were streaked onto M9 salts + 1 mg mL^{-1} nicotine plates to examine for growth. Only the WT grew well on these plates. WT and *cycN* strains were grown overnight in LB media and electroporated with pJN105 empty vector and pJN105-*cycN* for the complementation assay. These were plated onto LB + 25 μg mL^{-1} gentamycin selection plates. Single colonies from these plates were then streaked onto fresh plates containing M9 salts + 1 mg mL^{-1} nicotine additionally supplemented with 25 μg mL^{-1} gentamycin and 0.01% arabinose to observe for growth at 30 °C for 2–5 days.

In vitro assays.

The buffer used in all *in vitro* experiments was 40 mM HEPES-KOH, pH 7.5, 100 mM NaCl, 10% glycerol. NicA2 is in its fully oxidized form under ambient conditions in the absence of nicotine. The absorbance spectrum of oxidized FAD was used to determine the concentration of NicA2, using an extinction coefficient of 11,300 M^{-1} cm^{-1} at 450 nm. 20 μM NicA2 was combined with 40 μM nicotine and rapidly transferred to an absorbance cuvette to measure reduction of NicA2 under ambient conditions.

CycN was fully oxidized by addition of 5 mM ferricyanide. Excess ferricyanide was then exchanged out of the sample by running over a PD-10 desalting column before use. Concentrations of CycN were determined using the extinction coefficient of oxidized cytochrome c at 410 nm (101,600 M^{-1} cm^{-1}). NicA2 and CycN were observed for characteristic spectrophotometric changes in a Shimadzu UV-1900 UV-vis spectrophotometer. 3.75 μM CycN was combined with either 100 μM nicotine alone, 30 nM NicA2 alone, or both together and monitored for change between 250–600 nm. The same assay was performed with bovine cytochrome c (Sigma-Aldrich), except that the concentration of bovine cytochrome c was 6.84 μM. It was monitored for change in absorbance in the same region (250–600 nm) for 15 min. Oxidized CycN was additionally titrated with increasing amounts of sodium dithionite to achieve a fully reduced state, with absorbance scans taken at each titration step.

Nicotine degradation assay.

This assay was performed to determine both the amount of nicotine degraded and the concentration of NicA2 enzyme in cultures of *P. putida* S16 grown in the presence of nicotine. Both wild-type and *cycN* strains were grown overnight in LB. The next day, these cultures were diluted to OD 0.1 in 5 mL M9 salts + 0.4% glycerol and allowed to grow for 2 h. At this time point, nicotine was added to a final concentration of 1 mg mL^{-1} in each sample. The point of nicotine addition was considered time = 0. From then on, the cultures were sampled at 2, 4, 8,16, and 24 h. 200 μL of culture extracted at each time point was spun down at 16,000*g* for 10 min. The supernatant was isolated, and 100 μL supernatant was mixed with 300 μL methanol to prepare HPLC samples. The cell pellet was resuspended in 100 μL Bacterial Protein Extraction Reagent (B-PER; Thermo Fisher) and allowed to incubate at room temperature for 15 min to complete lysis. After this time had elapsed, 25 μL of 5x reducing gel loading buffer was added to each sample.

Samples for HPLC were further clarified by spinning at 16,000*g* for 30 min. 100 μL of each clarified sample was placed into autosampler vials. These were injected then separated for analysis using a Vydac C18 4.6×250 mm column (Catalog: 218TP54) and an isocratic water + 0.1% TFA mobile phase. A nicotine standard concentration gradient from 10 mM down to 1 μM was run. 10 μL of standards and experimental samples were injected for analysis. Samples and standards were within the linear range of detection, and the absorbance peaks were integrated for quantification.

Samples for western blot analysis were boiled for 5 min. Protein standards of purified NicA2 were prepared at known concentrations from 1 μM to 1 nM. 10 μL of each sample and

standard were loaded onto a Bio-Rad 12% SDS-reducing gel and run at 150 V until
completion. The gel was transferred to nitrocellulose blot via the Trans-Blot Turbo system
(Bio-Rad). Blots were blocked in 5% milk TBST and stained with 1:10,000 rabbit-derived
NicA2 antisera (Pacific Immunology) overnight at 4 °C. Blots were washed with 5% milk
TBST three times, and then incubated with 1:20,000 goat anti-rabbit IR800 dye (LI-COR
Biosciences) for 2 h at room temperature. Membranes were washed with TBST and then
imaged using a LI-COR Odyssey Clx. Protein bands were quantified using LI-COR Odyssey
software, and the NicA2 standard curve was used to determine the linear range of detection
and concentration of NicA2 at each time point from the experiment.

Sedimentation velocity analytical ultracentrifugation (SV-AUC).

SV-AUC was carried out using 400 μl sample loaded into two-sector titanium centerpieces
with 1.2 cm path-length in an An60Ti rotor in a Beckman Optima Xl-I analytical
ultracentrifuge. Measurement was completed in intensity mode. All SV-AUC data were
analyzed using UltraScan 4 software, version 4.0 and fitting procedures were completed on
XSEDE clusters at the Texas Advanced Computing Center (Lonestar, Stampede) through the
UltraScan Science Gateway (https://www.xsede.org/web/guest/gateways-listing)[41]. The
partial specific volume (vbar) of NicA2 was estimated within UltraScan III based on the
protein sequence[42]. Raw intensity data were converted to pseudo-absorbance by using the
intensity of the air above the meniscus as a reference and edited. 2-dimensional
sedimentation spectrum analysis (2DSA) was performed to subtract time-invariant noise and
the meniscus was fit using ten points in a 0.05-cm range[43]. First arrays with a broad S range
were fitted to account for possible large oligomeric states. Final arrays were fit using an S
range 1–10, an f/f0 range of 1–4 with 64 grid points for each, 10 uniform grid repetitions
and 400 simulation points. 2DSA was then repeated at the determined meniscus to fit
radially invariant and time-invariant noise together using ten iterations. The 2DSA solution
was refined by a genetic algorithm (GA), which uses an evolutionary based approach using
random cross-over, mutations and deletion operations to alter the solute characteristics of the
2DSA solutes to eliminate false positive solutions[44]. The results from the genetic algorithm
were evaluated using a Monte Carlo algorithm.

Transient kinetics.

All stopped-flow experiments were performed in 40 mM HEPES-KOH, pH 7.5, 100 mM
NaCl, 10% glycerol at 4 °C. NicA2 and CycN solutions were made anaerobic in glass
tonometers by repeated cycles with vacuum and anaerobic argon[45]. When needed, NicA2's
FAD was reduced in the anaerobic tonometer by titrating with a dithionite solution or
anaerobic nicotine solution housed in a gas-tight Hamilton syringe. The dithionite or
nicotine solutions were slowly added up to the point where NicA2's flavin reached the fully-
reduced hydroquinone state, and the redox status of the flavin was spectrophotometrically
monitored during the titration using a Shimadzu UV-1900 UV-vis spectrophotometer (UV
Probe software). Nicotine-containing buffer solutions were made anaerobic by sparging for
at least 10 min with anaerobic argon. Buffer containing O_2 at specific concentrations was
prepared by sparging different O_2/N_2 gas ratios through buffer in a gas-tight syringe for at
least 15 min at room temperature. The various O_2/N_2 gas ratios were prepared from O_2 and

N$_2$ gas cylinders using a Maxtec MaxBlend 2 gas mixer, and the dissolved O$_2$ concentration in the buffer solution was calculated using a Henry's law constant for O$_2$ of 770 atm M^{-1}.

Stopped-flow experiments were conducted using a TgK Scientific SF-61DX2 KinetAsyst stopped-flow instrument (with Kinetic Studio software) that had been previously equilibrated with a glucose/glucose oxidase solution to make the internal components of the system anaerobic. ~30 μM NicA2 (flavin concentration before mixing) was loaded onto the instrument and mixed with substrate (nicotine, O$_2$, or CycN) at a range of concentrations. The reactions were monitored either using the instrument's multi-wavelength CCD detector (1.6 ms data interval time) or a single wavelength detector with photomultiplier tube. Kinetic traces were fit to sums of exponentials using KaleidaGraph (Synergy Software) to determine observed rate constants.

Steady state assays.

Anaerobic steady state assays were performed in a stopped-flow spectrophotometer in 40 mM HEPES-KOH, pH 7.5, 100 mM NaCl, 10% glycerol at 4 °C. NicA2 and nicotine were made anaerobic in a glass tonometer with the nicotine in a side arm separated from the NicA2 solution. After achieving anaerobiosis, the nicotine was added to the NicA2 solution, resulting in a solution containing 200 nM NicA2 (flavin concentration) and 2 mM nicotine. The NicA2/nicotine solution was then mixed with various concentrations (10–255 μM before mixing) of anaerobic, oxidized CycN and the reduction of CycN was observed at 550 nm over 80 s. The linear rate was obtained over the first 5 s of the reaction and 21,000 M^{-1}cm^{-1} was used as the difference in extinction coefficient at 550 nm between reduced and oxidized CycN[46].The rate data were divided by two since two CycN molecules are used in a single turnover by NicA2 and then divided by the NicA2 concentration (100 nM after mixing in the experiment) to obtain the apparent turnover number for each CycN concentration.

Amplex Red Assay.

For H$_2$O$_2$ detection, these assays were performed similarly to what has been previously reported for NicA2[9,15] following the recommendations provided in the Amplex Red Assay Kit (Thermo Fisher Scientific). Assays were performed in 40 mM HEPES-KOH, pH 7.5, 100 mM NaCl. Reactions were measured in a platereader with excitation wavelength of 530 nm and emission wavelength of 590 nm. Samples were combined to have end concentrations of the following constituents in a 100 μL reaction: 1 μM NicA2 (flavin concentration), 20 μM oxidized CycN, 10 μM nicotine, 0.1 units mL^{-1} horseradish peroxidase, 50 μM Amplex Red. These were mixed and immediately observed at room temperature in the plate reader for 30 min. A standard curve of H$_2$O$_2$ stock concentrations was used to determine the linear range of the assay and assign the concentration of H$_2$O$_2$ produced in each case.
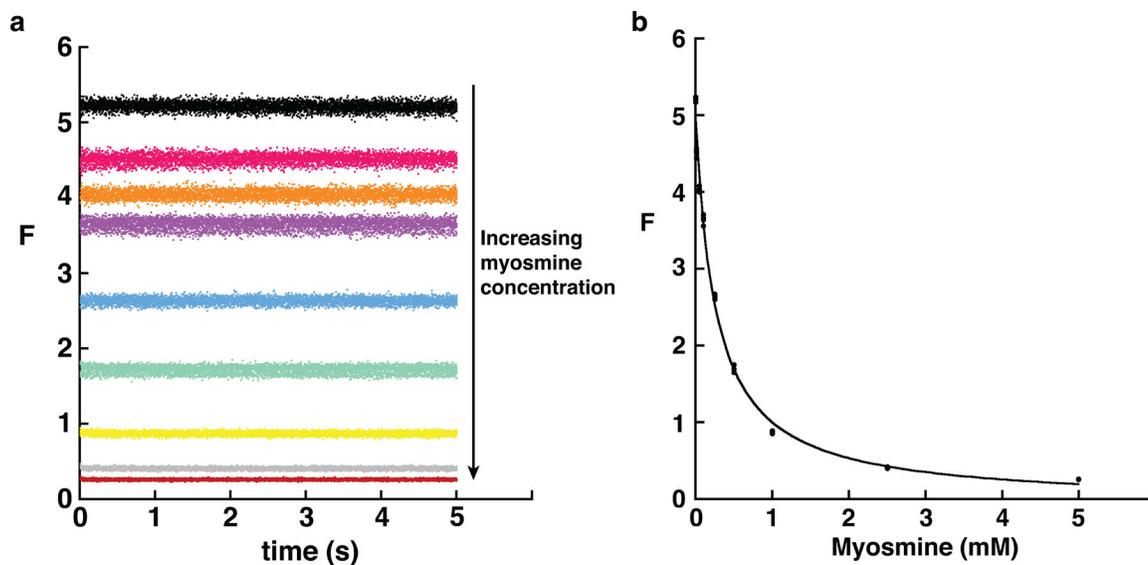
Extended Data
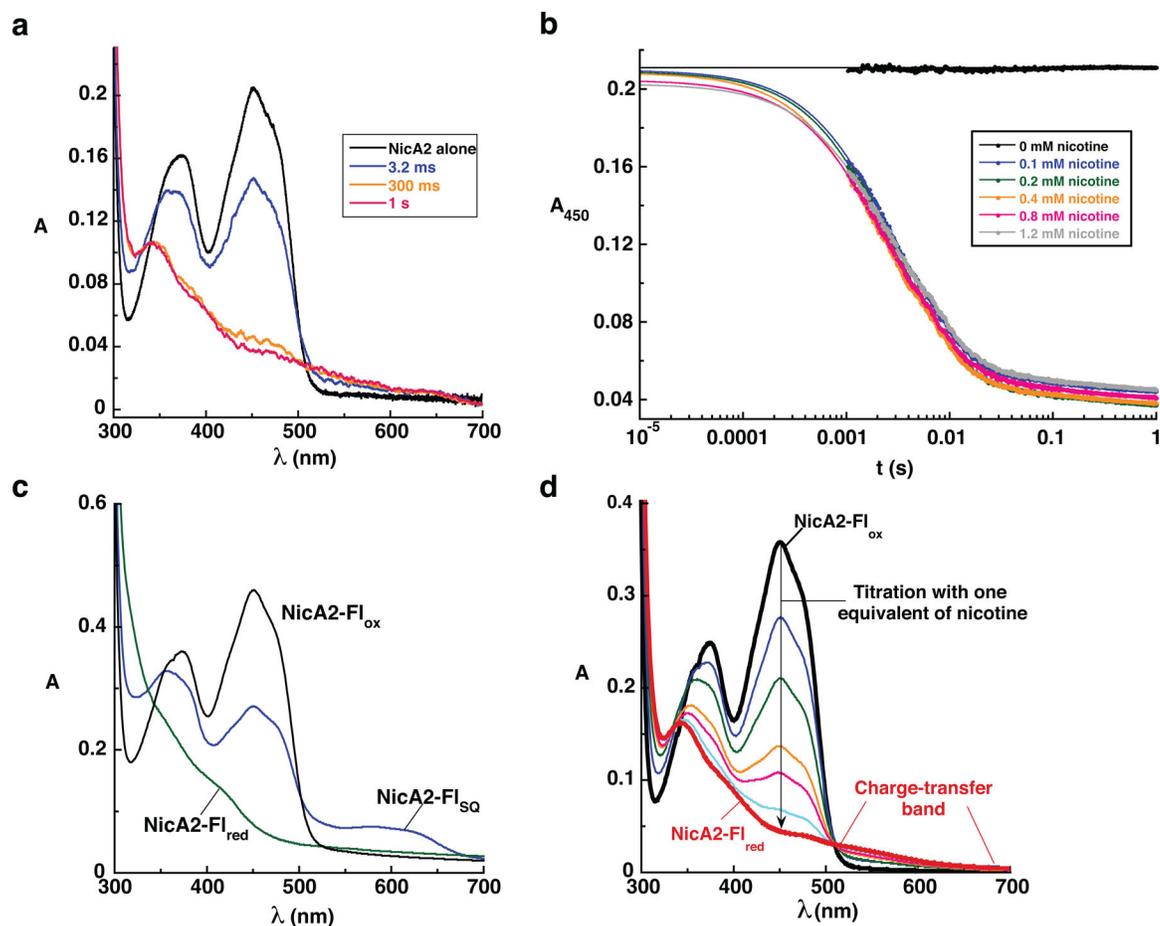
Extended Data Fig. 1. Reduction of NicA2 by nicotine, absorbance traces and intermediates.
a, Oxidized NicA2 was rapidly mixed with 0.2 mM nicotine and absorption of its flavin cofactor monitored using a CCD detector. The two intermediates detectable in reaction traces at 450 nm were maximally populated at 3.2 and 300 ms, and the absorbance spectra at these two points is shown. **b,** Absorbance trace overlay at 450 nm from stopped-flow experiments where NicA2 was reduced by rapid mixing with various concentrations of nicotine. Traces at all nicotine concentrations extrapolated back to the absorbance of NicA2-Fl_{ox} at time zero, indicating that no observable kinetic events were missed within the dead time of the stopped-flow instrument. Note the logarithmic timescale. **c,** Partial reduction of oxidized NicA2 with sodium dithionite produced a species with an increased absorbance from 525–650 nm. The spectrum of the titration point with the highest absorbance in this region is most consistent with a mixed population of oxidized flavin, flavin hydroquinone, and neutral flavin semiquinone[19]. Further titration with sodium dithionite resulted in complete reduction to the hydroquinone ($FADH_2$) state. NicA2-Fl_{ox}, NicA2 containing oxidized FAD; NicA2-Fl_{red}, NicA2 containing $FADH_2$; NicA2-Fl_{SQ}, NicA2 containing flavin semiquinone. **d,** NicA2-Fl_{ox} was reduced by titration of one molar equivalent of nicotine, resulting in reduction of the flavin cofactor as monitored by absorbance. Additionally, a charge transfer band developed in the region of 500–700nm over the course

of the titration, likely indicating that at least some amount of N-methylmyosmine product remains bound to NicA2 after reduction of its flavin.
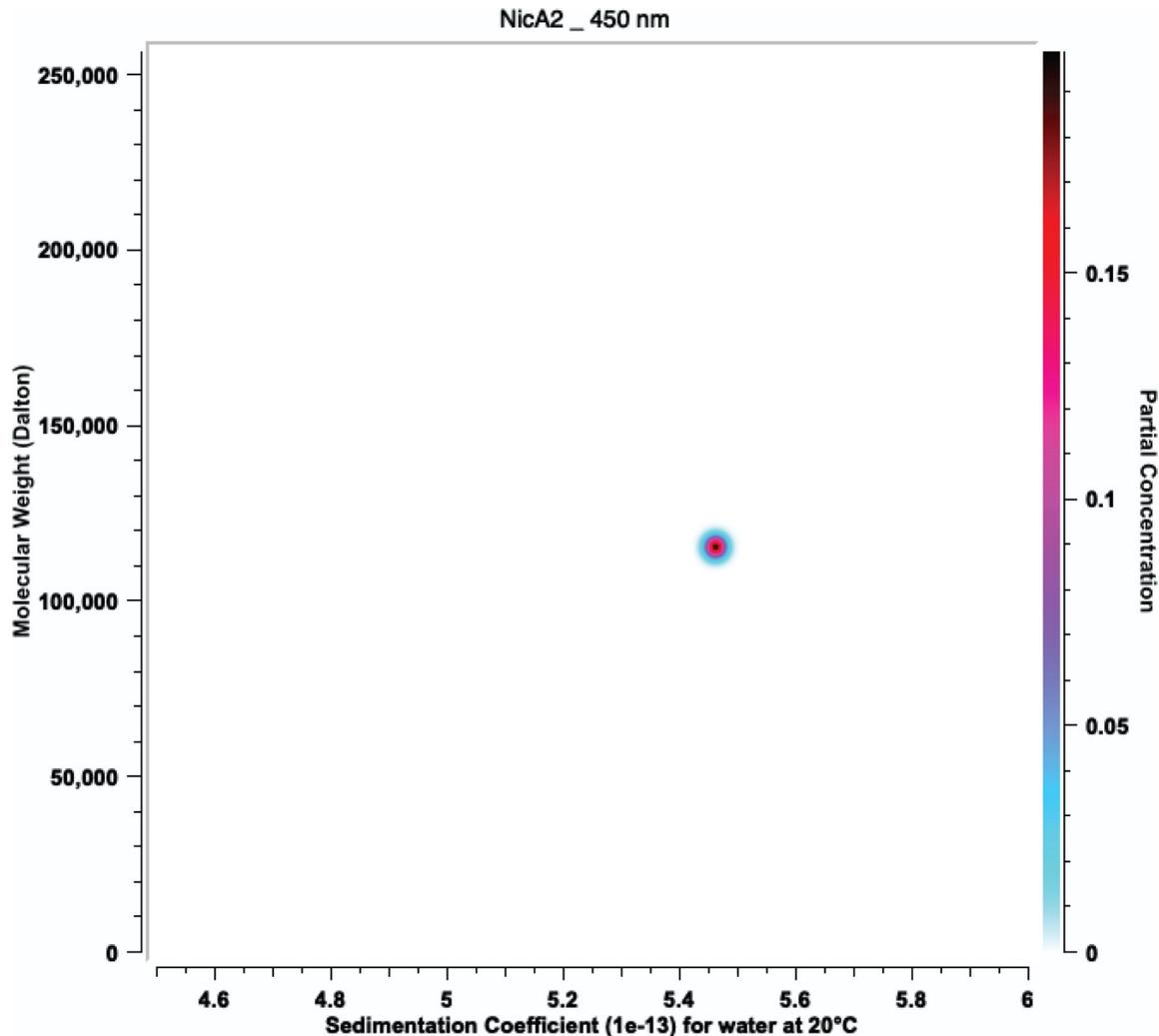

Extended Data Fig. 2. NicA2 is a dimer in solution.
Previous work has described NicA2 as a monomer using size exclusion chromatography[14,15]. To determine the quaternary structure of NicA2 in our buffer conditions, a solution of NicA2 at 20 μM (monomer concentration) was subjected to analysis by sedimentation velocity AUC at a rotor speed of 44,000 rpm while monitoring 450 nm. Data were analyzed using UltraScan 4, version 4.0. One species predominated in solution, with a sedimentation coefficient of ~5.45 and an apparent molecular weight of ~115 kDa. The expected molecular weight for the NicA2 monomer is 53.13 kDa, indicating that NicA2 is a homodimer in solution under these conditions. This experiment was independently repeated twice with similar results.

Extended Data Fig. 3. NicA2 rapidly forms a complex when titrated with the non-catalytic nicotine analogue myosmine.

a, Tryptophan fluorescence was used to quantify binding of myosmine as previously performed[9]. Traces from a stopped-flow experiment where oxidized NicA2 was mixed with varying concentrations of myosmine demonstrate a rapid binding event, occurring within the dead time (1 ms) of the instrument. **b,** Averaged fluorescence values of 5 traces per myosmine concentration were fit to determine the K_d for myosmine binding at 268 ± 3 μM (s.e.m.).

a

b

c

d

e
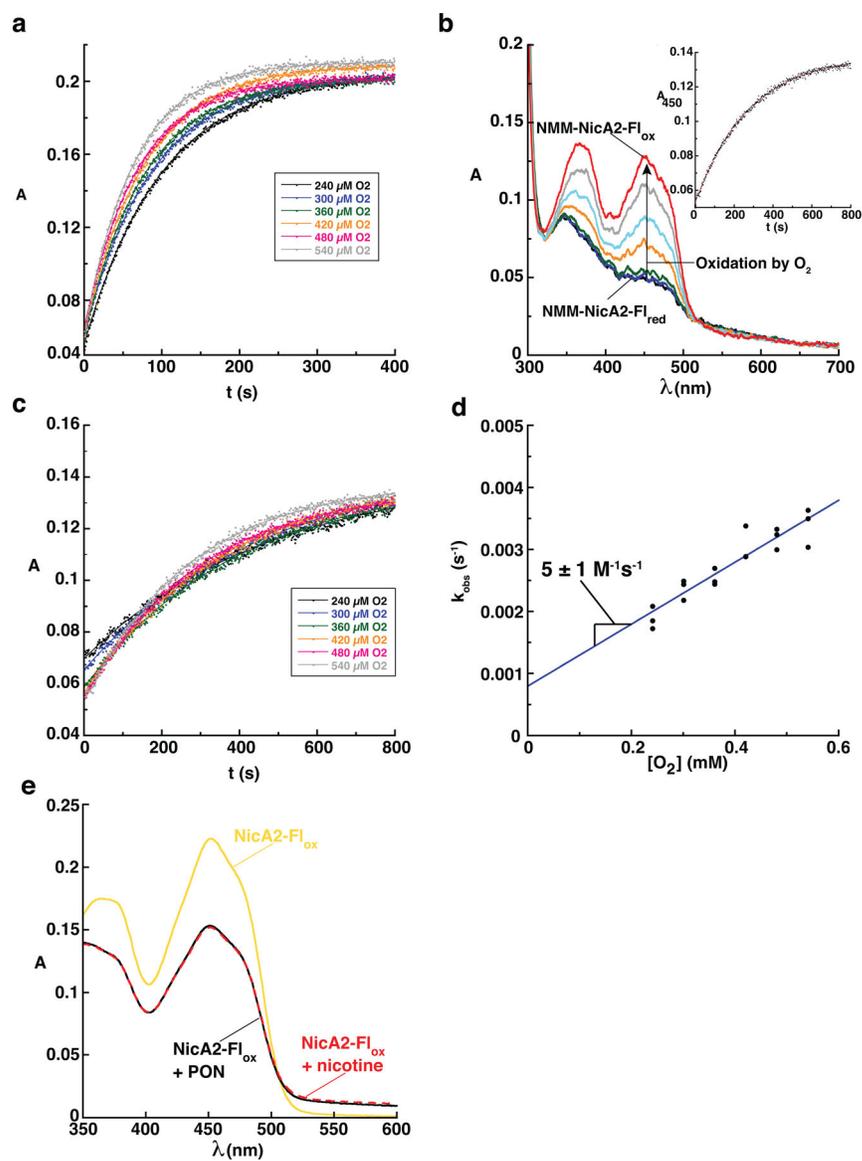
Extended Data Fig. 4. NicA2 is slowly re-oxidized by O_2 in the presence and absence of N-methyl-myosmine.

a, Absorbance traces from stopped-flow experiments where NicA2, first reduced with dithionite, was then rapidly mixed with variable concentrations of O_2. **b,** NicA2 was reduced with an equimolar amount of nicotine, and then rapidly mixed with O_2 in a stopped-flow experiment which was monitored via the CCD detector. Inset: following the absorbance at 450nm over time in this experiment, re-oxidation was very slow, similar to the behavior of dithionite reduced NicA2. NMM-NicA2-Fl_{ox}, N-methylmyosmine bound NicA2 containing oxidized flavin; NMM-NicA2-Fl_{red}, N-methylmyosmine bound NicA2 containing reduced flavin. **c**, Absorbance traces from stopped-flow experiments where NicA2, first reduced with nicotine, resulting in NMM-NicA2-Fl_{red}, was then rapidly mixed with variable concentrations of O_2. **d,** k_{obs} values for the re-oxidation of NMM-bound NicA2 were plotted against the concentration of O_2, demonstrating linear dependence. **e,** The absorbance spectrum of NicA2-Fl_{ox} (yellow) was compared in two conditions. In one case (red dashed

line), nicotine was added to 40 μM end concentration, and the reaction allowed to proceed for 30 minutes until complete re-oxidation of the flavin. In the other case (black solid line) pseudooxynicotine was added to an end concentration of 40 μM and the spectrum taken immediately. NicA2-Fl$_{ox}$, NicA2 containing oxidized flavin; PON, pseudooxynicotine. These experiments were independently repeated twice with similar results. Values reported are the mean ± s.e.m. of the fit.
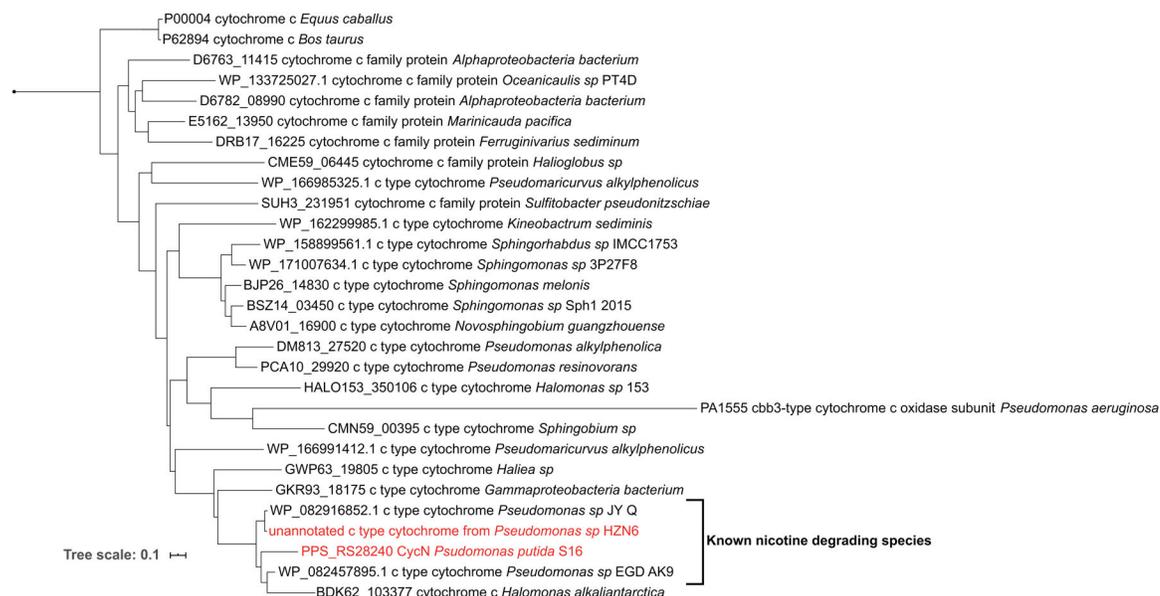
Extended Data Fig. 5. CycN is most closely related to cytochromes from other nicotine degrading species.

CycN (highlighted in red) was used as the template for an NCBI BLAST homology search. The sequences with highest homology were collected, and identical sequences removed. A tree was generated using the NGPhylogeny web server with default settings[48], then formatted into a figure using the Interactive Tree of Life (iTOL)[49]. Notably, the cytochrome c from *Pseudomonas sp.* HZN6[50] (highlighted in red) is not included in the NCBI database, but was added to the sequence set after manual review of that organisms genome. It appears that other known nicotine degrading organisms also contain cytochromes c similar to CycN, suggesting that they use a similar electron transfer pathway[50,51]. Sequence analyses of CycN related sequences was complicated by the fact that there is relatively poor annotation of these proteins in nicotine degrading organisms. For example, manual review of the pyrrolidine-pathway nicotine degrading bacteria *Pseudomonas sp.* HZN6 revealed an unannotated cytochrome c homologous protein just downstream of nicotine oxidoreductase. This is the same genomic architecture as for *P. putida* S16. This poor annotation led us to manually review other nicotine degrading organism's genomes, in which we identify a consistent pattern. In organisms that use the pyrrolidine pathway, like *P. putida* S16, there are nicotine oxidoreductase enzymes similar to NicA2 with neighboring cytochrome c proteins. In those that metabolize nicotine via the pyridine pathway, there do not appear to be protein-based electron acceptors in the region of their nicotine degrading enzymes. For variant pyrrolidine/pyridine pathway (VPP) organisms, these do not appear to have cytochromes c, but often have pseudoazurin proteins in their nicotine degrading genomic

islands. Pseudoazurins are able to participate in a range of electron transport reactions in the periplasm of bacteria[52], though it is unclear if they could serve this role for flavin dependent amine oxidases in these organisms.
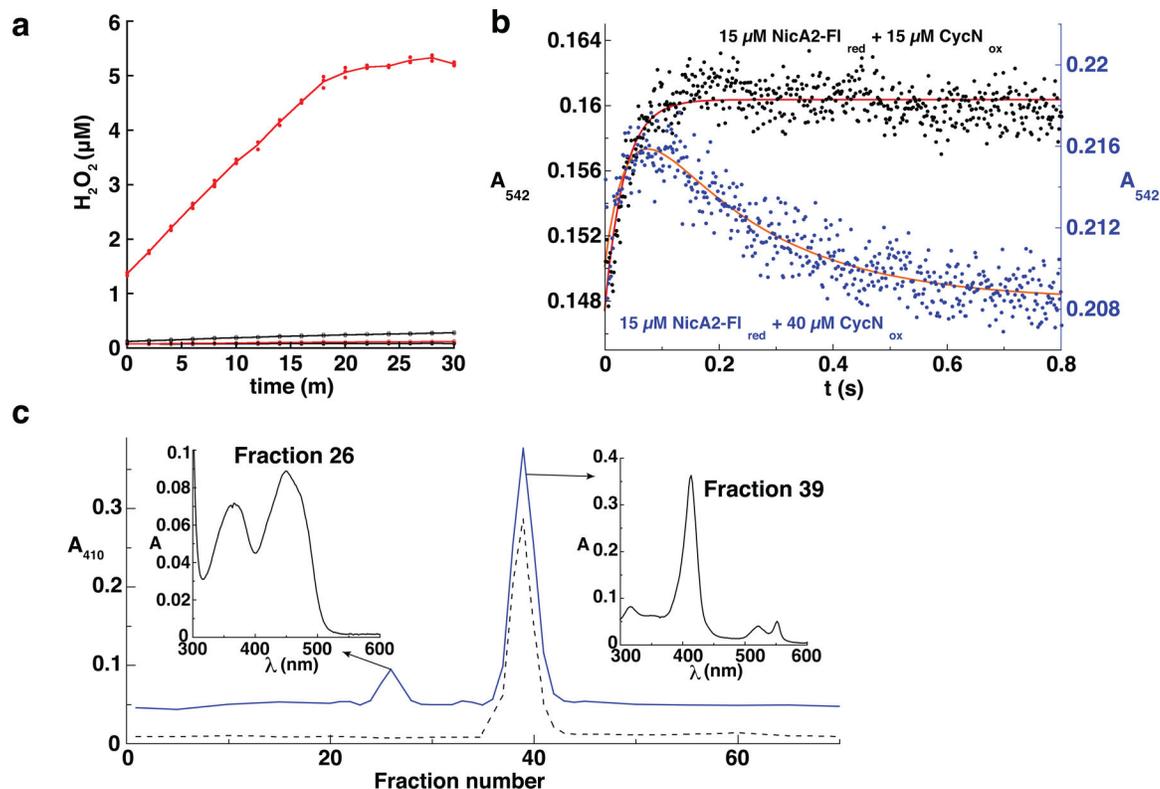
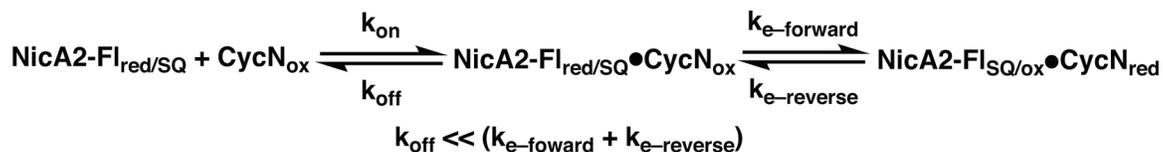**Extended Data Fig. 6. NicA2 and CycN's interaction.**

a, Oxidized NicA2 was incubated with nicotine under aerobic conditions in the presence (black filled circles) and absence (red filled circles) of oxidized CycN, and the amount of H_2O_2 produced by the reaction was monitored using the Amplex Red assay. Also included were conditions of NicA2 without nicotine (black empty circles) and with CycN but without nicotine (red empty circles). Only in the condition where NicA2 was incubated with nicotine in the absence of CycN was a significant amount of H_2O_2 produced. Three independent replicates were obtained and plotted. **b**, Oxidized CycN and reduced NicA2 were combined in an anaerobic stopped-flow spectrophotometer and observed for change in absorbance at 542 nm. When mixed in equimolar amounts (black points), absorbance rose and was maintained at an increased value indicating transition to the flavin semiquinone state. When mixed with excess CycN (blue points), NicA2 first reaches the semiquinone state (observable as an increase in absorbance) before becoming fully oxidized (observable as a subsequent decrease in absorbance). **c,** 40 μM CycN alone (black dashed line) or 40 μM CycN with 200 μM NicA2 (blue line) were run over a HiLoad Superdex 75 pg size exclusion column. CycN in the presence of excess NicA2 eluted with the same retention time as CycN alone and was well-resolved from the NicA2 peak. The insets show the absorbance spectrum of the two peaks in the chromatogram. Fractions 26 and 39 have

spectra consistent with clean NicA2 and CycN, respectively, indicating that the two proteins do not bind with high affinity.
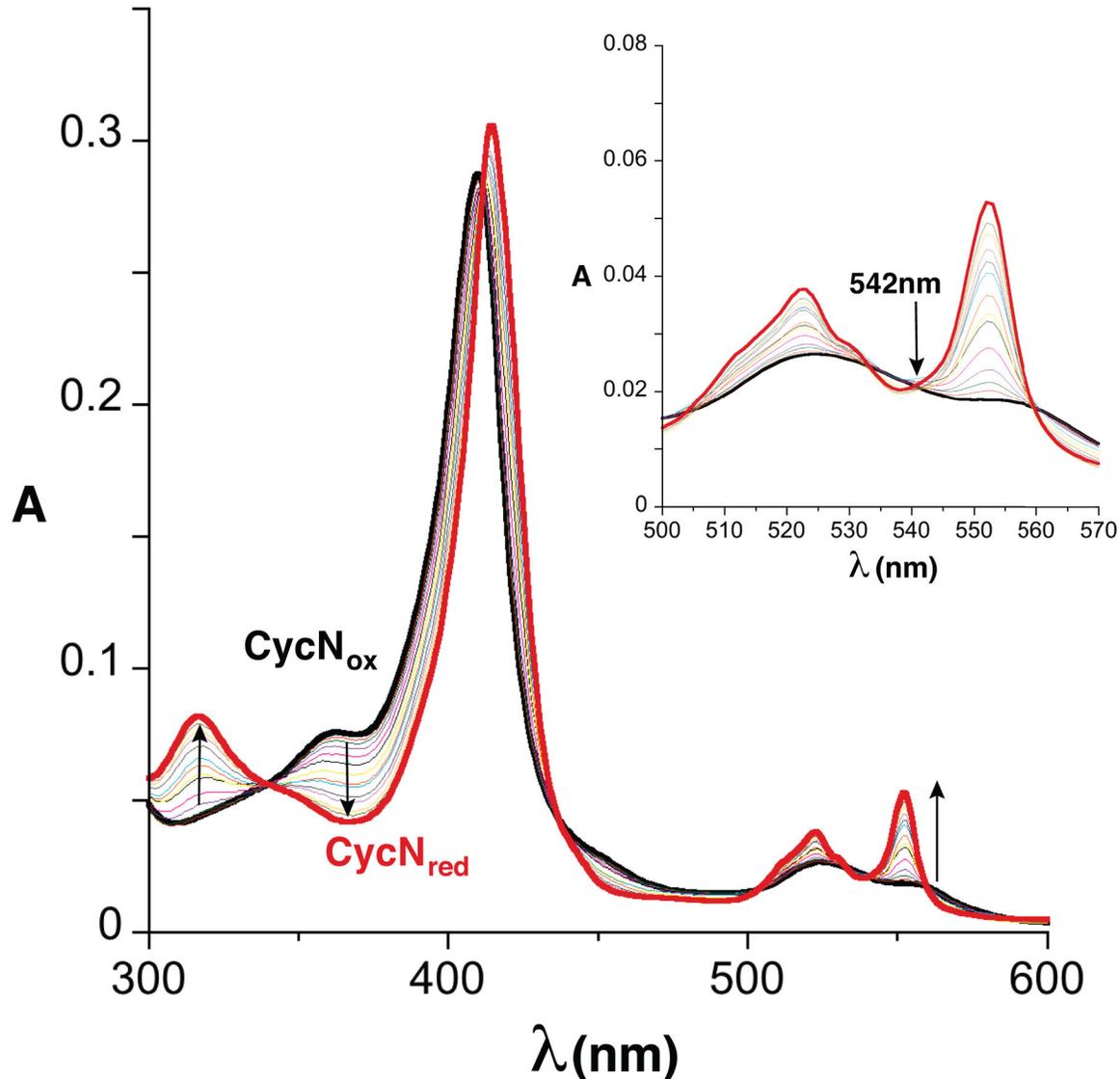
Extended Data Fig. 7. Reduction of CycN by dithionite.
UV-VIS spectra were recorded as sodium dithionite was serially titrated into a solution of oxidized CycN until it became fully reduced. Arrows represent the directionality of change during the titration. Inset: zooming in on just a small section of this titration, an isosbestic point is visible at 542 nm marked with an arrow. This wavelength was used to monitor the changes in absorbance for NicA2's FAD in the experiments in Fig. 4.

$$\text{NicA2-Fl}_{red/SQ} + \text{CycN}_{ox} \underset{k_{off}}{\overset{k_{on}}{\rightleftharpoons}} \text{NicA2-Fl}_{red/SQ} \bullet \text{CycN}_{ox} \underset{k_{e-reverse}}{\overset{k_{e-forward}}{\rightleftharpoons}} \text{NicA2-Fl}_{SQ/ox} \bullet \text{CycN}_{red}$$

$$k_{off} << (k_{e-foward} + k_{e-reverse})$$

Extended Data Fig. 8. Kinetic model for NicA2 oxidation by CycN.

In a two-step mechanism where rate-limiting $CycN_{ox}$ binding to $NicA2-Fl_{red}$ is followed by rapid electron transfer between the two redox centers, k_{obs} should be linearly dependent on $[CycN_{ox}]$ at low $CycN_{ox}$ concentrations and should saturate at the sum of the rate constants for electron transfer ($k_{e-forward} + k_{e-reverse}$) at high $CycN_{ox}$ concentrations[53]. Our data indicate that we have used $CycN_{ox}$ concentrations at the low end of this concentration regime, where k_{obs} increases linearly with $CycN_{ox}$ concentration with a slope equal to k_{on} for $CycN_{ox}$ binding to $NicA2-Fl_{red}$. We presume that k_{obs} would eventually reach a saturating value at high $CycN_{ox}$ concentrations; however, we are not able to produce enough $CycN_{ox}$ to explore the mM concentrations of $CycN_{ox}$ that would be needed to achieve saturation. Notably, the rate constant for $CycN_{ox}$ dissociation from $NicA2-Fl_{red}$ (k_{off}) should not contribute to the y-intercept of the k_{obs} plot for the mechanism shown in this figure[53]. The k_{obs} for the second phase also increased linearly with $CycN_{ox}$ concentration, indicating that the above logic also applies for the reaction of the second $CycN_{ox}$ with $NicA2-Fl_{SQ}$. This finding also indicates that $CycN_{red}$ resulting from the first one-electron transfer must dissociate from $NicA2-Fl_{SQ}$ fast enough such that the second one-electron transfer event is also rate-limited by $CycN_{ox}$ binding. In the kinetic scheme, the labels $NicA2-Fl_{red/SQ}$ and $NicA2-Fl_{SQ/ox}$ indicate that $NicA2-Fl_{red}$ conversion to $NicA2-Fl_{SQ}$ and $NicA2-Fl_{SQ}$ conversion to $NicA2-Fl_{ox}$ are observed in the first and second phases, respectively.
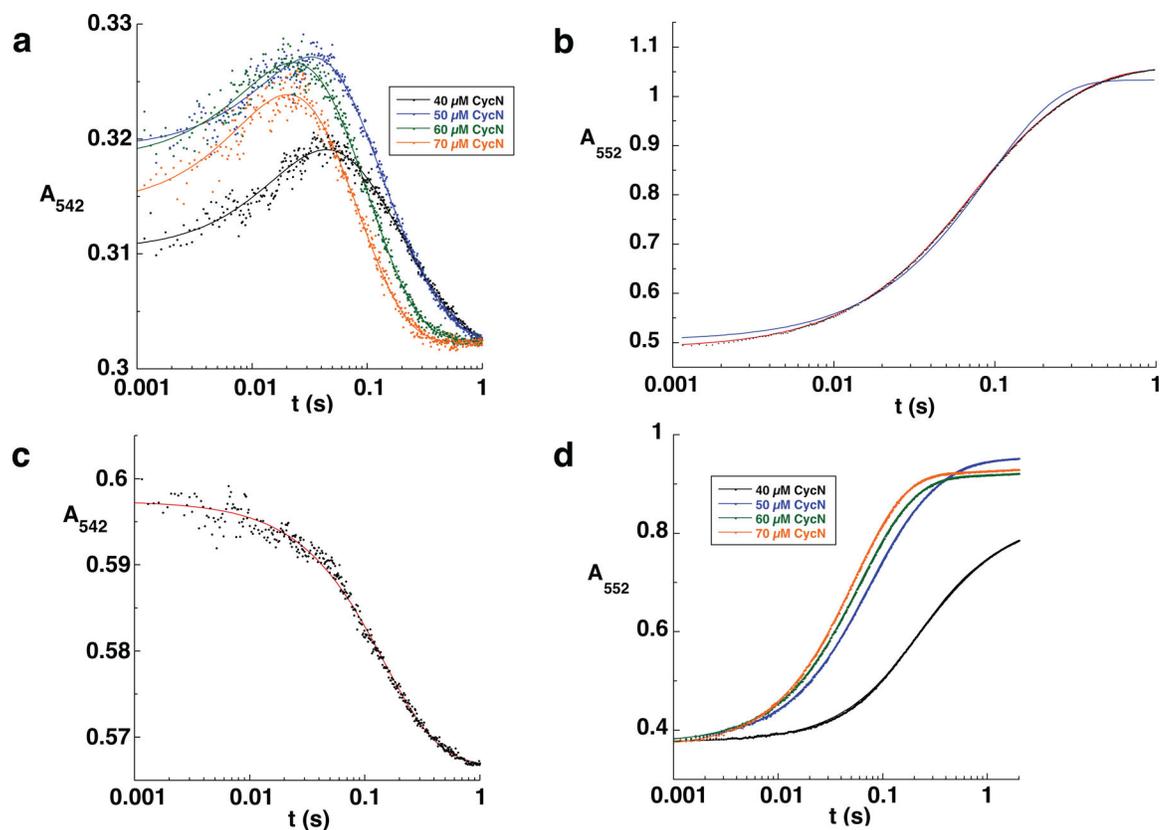
Extended Data Fig. 9. CycN stopped-flow data.

a, Absorbance traces for the stopped flow reaction between ligand-free $NicA2-Fl_{red}$ with variable concentrations of $CycN_{ox}$. In this case, the traces were able to capture formation

and depletion of NicA2-Fl$_{SQ}$ that occurred as the reaction proceeded. CycN contributes a substantial amount of absorbance at 542 nm. Accordingly, the traces were adjusted so that they all end at the same absorbance value to facilitate comparison. Note the logarithmic timescale. **b**, Signal change for the stopped-flow reaction was also monitored at 552 nm, a wavelength suitable for observing reduction of CycN. The trace required two exponentials (red curve) with similar amplitudes to fit properly, as one exponential (blue curve) was insufficient. Signal change occurred at the same time as NicA2 oxidation monitored at 542 nm, indicating that the processes occurred simultaneously. Note the logarithmic timescale. **c,** Signal change at 542 nm for the reaction of NMM-NicA2-Fl$_{red}$ with CycN$_{ox}$. Curiously, traces at 542 nm, where NicA2-Fl$_{SQ}$ is detectable, did not show the increase in absorbance that we observed with ligand-free NicA2-Fl$_{red}$; traces at this wavelength showed a decrease in absorbance that occurred in two phases, with the first phase contributing 80–90% of the total absorbance. This observation suggests that N-methylmyosmine in the active site inhibits NicA2's FAD from populating a semiquinone state during the reaction with CycN. The decrease in absorbance at 542 nm may simply be due the small decrease in charge-transfer absorbance of N-methylmyosmine bound NicA2 that occurs when the flavin gets oxidized (Extended Data Fig. 4b). Reaction traces at 552 nm still showed the two kinetic phases with increasing absorbance (Extended Data Fig. 9b). Note the logarithmic timescale. **d,** Absorbance traces at 552 nm for the stopped flow reaction between NMM-NicA2-Fl$_{red}$ and variable concentrations of CycN$_{ox}$. Traces fit best to two exponentials and the k$_{obs}$ values are reported in Fig. 4c of the main text. The traces were adjusted so that they all begin at the same absorbance value for comparison. Note the logarithmic timescale.
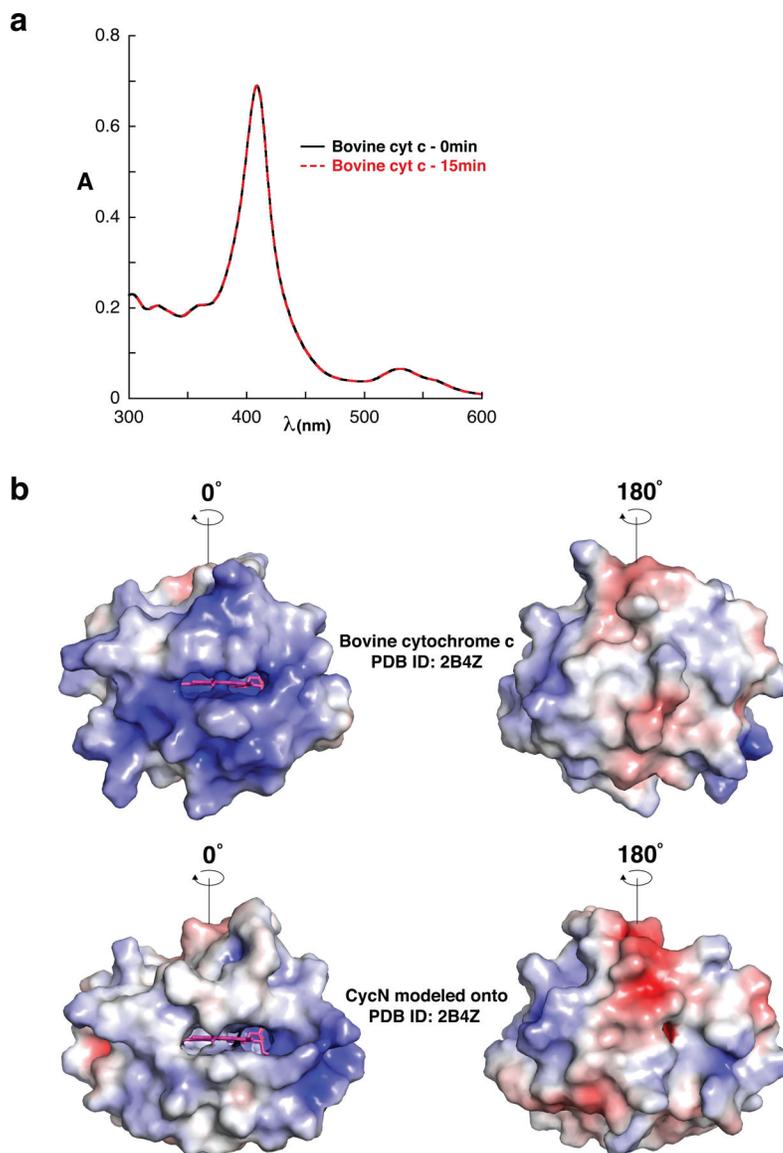
Extended Data Fig. 10. Bovine cytochrome c is not reduced by NicA2 and has different surface charge distribution than CycN.

a, Bovine cytochrome c combined with nicotine and NicA2 did not result in any reduction of the cytochrome c over 15 min of incubation, unlike the assay performed with CycN (Fig. 3).

b, CycN was modeled onto the structure of bovine cytochrome c (PDB ID: 2B4Z) using the SWISS-MODEL online server[54]. Surface charge distribution of CycN and bovine cytochrome c was calculated using the APBS electrostatics plugin for PyMOL[55]. Bovine cytochrome c (top) is enriched for positive charge in the region where the heme is surface-exposed, whereas CycN (bottom) is closer to neutral/hydrophobic. Red color indicates negative charge density; blue color indicates positive charge density; heme cofactor is colored in magenta for both structures.

Supplementary Material

Refer to Web version on PubMed Central for supplementary material.

Acknowledgements

References

1. Massey V The chemical and biological versatility of riboflavin. Biochem. Soc. Trans 28, 283 (2000). [PubMed: 10961912]

2. El-Gebali S et al. The Pfam protein families database in 2019. Nucleic Acids Res. 47, D427–D432 (2019). [PubMed: 30357350]

3. Tararina MA & Karen NA Bioinformatic analysis of the flavin-dependent amine oxidase superfamily: adaptations for substrate specificity and catalytic diversity. J. Mol. Biol 432, 3269–3288 (2020). [PubMed: 32198115]

4. Fitzpatrick PF Oxidation of amines by flavoproteins. Arch. Biochem. Biophys 493, 13–25 (2010). [PubMed: 19651103]

5. Binda C, Mattevi A & Edmondson DE Structure-function relationships in flavoenzyme-dependent amine oxidations: a comparison of polyamine oxidase and monoamine oxidase. J. Biol. Chem 277, 23973–23976 (2002). [PubMed: 12015330]

6. Tang H et al. Novel nicotine oxidoreductase-encoding gene involved in nicotine degradation by pseudomonas putida strain S16. Appl. Environ. Microbiol 75, 772–778 (2009). [PubMed: 19060159]

7. Tang H et al. Systematic unraveling of the unsolved pathway of nicotine degradation in pseudomonas. PLoS Genet. 9, e1003923 (2013). [PubMed: 24204321]

8. Fitzpatrick PF The enzymes of microbial nicotine metabolism. Beilstein J. Org. Chem 14, 2295–2307 (2018). [PubMed: 30202483]

9. Tararina MA et al. Crystallography coupled with kinetic analysis provides mechanistic underpinnings of a nicotine-degrading enzyme. Biochemistry 57, 3741–3751 (2018). [PubMed: 29812904]

10. Xue S, Schlosburg JE & Janda KD A new strategy for smoking cessation: characterization of a bacterial enzyme for the degradation of nicotine. J. Am. Chem. Soc 137, 10136–10139 (2015). [PubMed: 26237398]

11. Pentel PR et al. The nicotine-degrading enzyme NicA2 reduces nicotine levels in blood, nicotine distribution to brain, and nicotine discrimination and reinforcement in rats. BMC Biotechnol. 18, 1–14 (2018). [PubMed: 29316906]

12. Thisted T et al. Optimization of a nicotine degrading enzyme for potential use in treatment of nicotine addiction. BMC Biotechnol. 19, 1–16 (2019). [PubMed: 30606176]

13. Kallupi M, Xue S, Zhou B, Janda KD & George O An enzymatic approach reverses nicotine dependence, decreases compulsive-like intake, and prevents relapse. Sci. Adv 4, eaat4751 (2018).

14. Tararina MA, Janda KD & Allen KN Structural analysis provides mechanistic insight into nicotine oxidoreductase from pseudomonas putida. Biochemistry 55, 6595–6598 (2016). [PubMed: 27933790]

15. Xue S et al. An enzymatic advance in nicotine cessation therapy. Chem. Commun 54, 1686–1689 (2018).

16. Kopacz MM, Heuts DPHM & Fraaije MW Kinetic mechanism of putrescine oxidase from rhodococcus erythropolis. FEBS J. 281, 4384–4393 (2014). [PubMed: 25060191]

17. Vintém APB, Price NT, Silverman RB & Ramsay RR Mutation of surface cysteine 374 to alanine in monoamine oxidase A alters substrate turnover and inactivation by cyclopropylamines. Bioorganic Med. Chem 13, 3487–3495 (2005).

18. Fitzpatrick PF, Chadegani F, Zhang S, Roberts KM & Hinck CS Mechanism of the flavoprotein l - hydroxynicotine oxidase: kinetic mechanism, substrate specificity, reaction product, and roles of active-site residues. Biochemistry 55, 697–703 (2016). [PubMed: 26744768]

19. Su D, Kabir MP, Orozco-Gonzalez Y, Gozem S & Gadda G Fluorescence properties of flavin semiquinone radicals in nitronate monooxygenase. ChemBioChem 20, 1646–1652 (2019). [PubMed: 30748074]

20. Mattevi A To be or not to be an oxidase: challenging the oxygen reactivity of flavoenzymes. Trends Biochem. Sci 31, 276–283 (2006). [PubMed: 16600599]

21. Yu H et al. Complete genome sequence of the nicotine-degrading pseudomonas putida strain S16. J. Bacteriol 193, 5541–5542 (2011). [PubMed: 21914868]

22. Almagro Armenteros JJ et al. SignalP 5.0 improves signal peptide predictions using deep neural networks. Nat. Biotechnol 37, 420–423 (2019). [PubMed: 30778233]

23. Lehninger AL, Nelson DL & Cox MM Lehninger Principles of Biochemistry. (W. H. Freeman, 2005).

24. Hmelo LR et al. Precision-engineering the pseudomonas aeruginosa genome with two-step allelic exchange. Nat. Protoc 10, 1820–1841 (2015). [PubMed: 26492139]

25. Leferink NGH, Van Den Berg WAM & Van Berkel WJH L-Galactono-γ-lactone dehydrogenase from arabidopsis thaliana, a flavoprotein involved in vitamin C biosynthesis. FEBS J. 275, 713–726 (2008). [PubMed: 18190525]

26. Kuwahara T, White RA & Agosin M A cytosolic flavin-containing enzyme catalyzing reduction of cytochrome c in trypanosoma cruzi: kinetic studies with cytochrome c as substrate. Arch. Biochem. Biophys 241, 45–49 (1985). [PubMed: 2992393]

27. Butt WD & Keilen D Absorption spectra and some other properties of cytochrome c and of its compounds with ligands. Proc. R. Soc. Lond. B. Biol. Sci 156, 429–458 (1962). [PubMed: 14040866]

28. Döpner S et al. The structural and functional role of lysine residues in the binding domain of cytochrome c in the electron transfer to cytochrome c oxidase. Eur. J. Biochem 261, 379–391 (1999). [PubMed: 10215847]

29. Kachalova GS et al. Crystal structure analysis of free and substrate-bound 6-hydroxy-l-nicotine oxidase from arthrobacter nicotinovorans. J. Mol. Biol 396, 785–799 (2010). [PubMed: 20006620]

30. Fitzpatrick PF, Chadegani F, Zhang S & Dougherty V Mechanism of flavoprotein l-6-hydroxynicotine oxidase: pH and solvent isotope effects and identification of key active site residues. Biochemistry 56, 869–875 (2017). [PubMed: 28080034]

31. Tang H et al. Molecular deceleration regulates toxicant release to prevent cell damage in Pseudomonas putida S16 (DSM 28022). MBio 11, 1–12 (2020).

32. Arai H Regulation and function of versatile aerobic and anaerobic respiratory metabolism in pseudomonas aeruginosa. Front. Microbiol 2, 1–13 (2011). [PubMed: 21716958]

33. Tribelli PM et al. Core regulon of the global anaerobic regulator Anr targets central metabolism functions in pseudomonas species. Sci. Rep 9, 1–13 (2019). [PubMed: 30626917]

34. Chaiyen P, Fraaije MW & Mattevi A The enigmatic reaction of flavins with oxygen. Trends Biochem. Sci 37, 373–380 (2012). [PubMed: 22819837]

35. Graves SM et al. Dopamine metabolism by a monoamine oxidase mitochondrial shuttle activates the electron transport chain. Nat. Neurosci 23, 15–20 (2020). [PubMed: 31844313]

36. Wang J & Edmondson DE Topological probes of monoamine oxidases A and B in rat liver mitochondria: Inhibition by TEMPO-substituted pargyline analogues and inactivation by proteolysis. Biochemistry 50, 2499–2505 (2011). [PubMed: 21341713]

37. Zhuang Z, Marks B & McCauley RB The insertion of monoamine oxidase A into the outer membrane of rat liver mitochondria. J. Biol. Chem 267, 591–596 (1992). [PubMed: 1309756]

38. Russell SM, Davey J & Mayer RJ The vectorial orientation of human monoamine oxidase in the mitochondrial outer membrane. Biochem. J 181, 7–14 (1979). [PubMed: 486161]

39. Gaweska H & Fitzpatrick PF Structures and mechanism of the monoamine oxidase family. 2, 365–377 (2012).

40. Londer YY Expression of recombinant cytochromes c in E. coli. Methods Mol. Biol 705, 123–150 (2011). [PubMed: 21125384]

41. Demeler B & Gorbet GE Analytical ultracentrifugation data analysis with UltraScan-III in Analytical Ultracentrifugation: Instrumentation, Software, and Applications (eds. Uchiyama S, Arisaka F, Stafford WF & Laue T) 119–143 (Springer Japan, Tokyo, 2016).

42. Demeler B, Brookes E & Nagel-Steger LBT-M in E. Chapter 4 Analysis of heterogeneity in molecular weight and shape by analytical ultracentrifugation using parallel distributed computing in Computer Methods, Part A 454, 87–113 (Academic Press, 2009).

43. Brookes E, Cao W & Demeler B A two-dimensional spectrum analysis for sedimentation velocity experiments of mixtures with heterogeneity in molecular weight and shape. Eur. Biophys. J 39, 405–414 (2010). [PubMed: 19247646]

44. Brookes E & Demeler B Genetic algorithm optimization for obtaining accurate molecular weight distributions from sedimentation velocity experiments in Analytical Ultracentrifugation VIII 33–40 (Springer-Verlag, Berlin, 2006).

45. Moran GR Anaerobic methods for the transient-state study of flavoproteins: the use of specialized glassware to define the concentration of dioxygen. Methods Enzymol. 620, 27–49 (2019) [PubMed: 31072490]

46. Zabinski-Snopko RM & Czerlinski GH Spectrophotometric titrations of ferricytochrome c with ferrohexacyanide in the pH range 5 to 7. J. Biol. Phys 9, 155–167 (1981).

47. Su D, Kabir MP, Orozco-Gonzalez Y, Gozem S & Gadda G Fluorescence properties of flavin semiquinone radicals in nitronate monooxygenase. ChemBioChem 20, 1646–1652 (2019). [PubMed: 30748074]

48. Lemoine F et al. NGPhylogeny.fr: New generation phylogenetic services for non-specialists. Nucleic Acids Res. 47, W260–W265 (2019). [PubMed: 31028399]

49. Letunic I & Bork P Interactive Tree of Life (iTOL) v4: Recent updates and new developments. Nucleic Acids Res. 47, 256–259 (2019).

50. Qiu J et al. Functional identification of two novel genes from Pseudomonas sp. Strain HZN6 involved in the catabolism of nicotine. Appl. Environ. Microbiol 78, 2154–2160 (2012). [PubMed: 22267672]

51. Li J et al. Comparative genomics reveals specific genetic architectures in nicotine metabolism of Pseudomonas sp. JY-Q. Front. Microbiol 8, 1–11 (2017). [PubMed: 28197127]

52. De Rienzo F, Gabdoulline RR, Menziani MC & Wade RC Blue copper proteins: A comparative analysis of their molecular interaction properties. Protein Sci. 9, 1439–1454 (2000). [PubMed: 10975566]

53. Bagshaw C Biomolecular Kinetics Ch 2.7: Two-step reversible binding reaction: inducted fit, 41–45 (CRC Press, Boca Raton, 2017).

54. Waterhouse A et al. SWISS-MODEL: Homology modelling of protein structures and complexes. Nucleic Acids Res. 46, W296–W303 (2018). [PubMed: 29788355]

55. Jurrus E et al. Improvements to the APBS biomolecular solvation software suite. Protein Sci. 27, 112–128 (2018). [PubMed: 28836357]
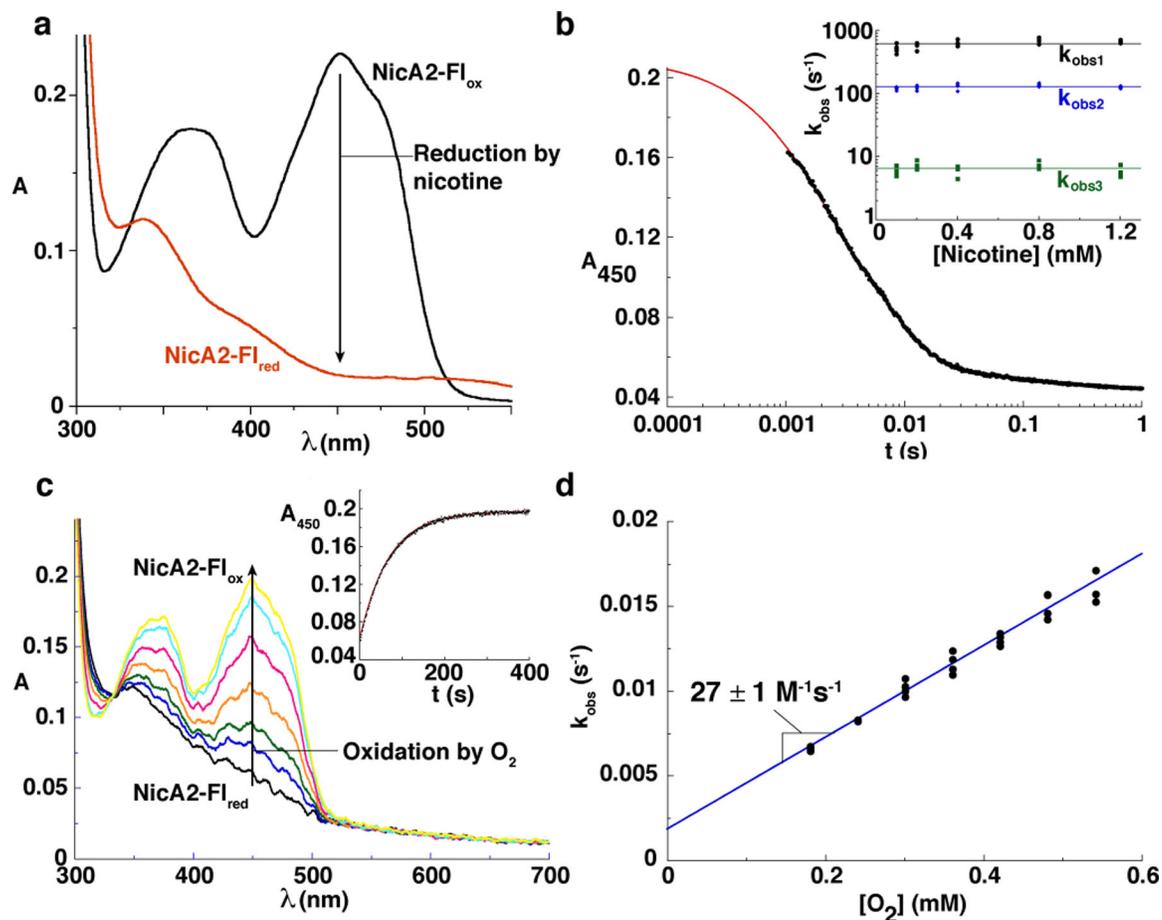
Figure 1 |. NicA2 is rapidly reduced by nicotine, but slowly re-oxidizes with O_2.
a, NicA2 under ambient conditions was monitored by UV-vis spectrophotometry in the region of FAD absorbance. Upon addition of nicotine, rapid and complete reduction of FAD was observed and sustained for several minutes. NicA2-Fl_{ox}, NicA2 containing oxidized FAD; NicA2-Fl_{red}, NicA2 containing $FADH_2$. **b**, Oxidized NicA2 was combined with varying concentrations of nicotine and the change in absorbance at 450 nm was monitored by anaerobic stopped-flow spectrophotometry. Note the logarithmic timescale. The resulting traces required three exponentials to fit properly. Inset: plotting the k_{obs} values of the three phases against the concentration of nicotine shows concentration independence. **c**, NicA2 was reduced by sodium dithionite titration under anaerobic conditions, then mixed with various concentrations of O_2 and monitored for the change in FAD absorbance by stopped-flow spectrophotometry. Inset: a representative trace showing re-oxidation of NicA2's FAD by 540 μM O_2 at 450 nm. See Extended Data Figure 4a for traces at other O_2 concentrations. These traces were well fit with a single exponential. **d**, The k_{obs} values derived from fitting re-oxidation traces were plotted against the O_2 concentration, demonstrating linear dependence. These experiments were independently repeated twice with similar results. Values reported are the mean ± s.e.m. of the fit.
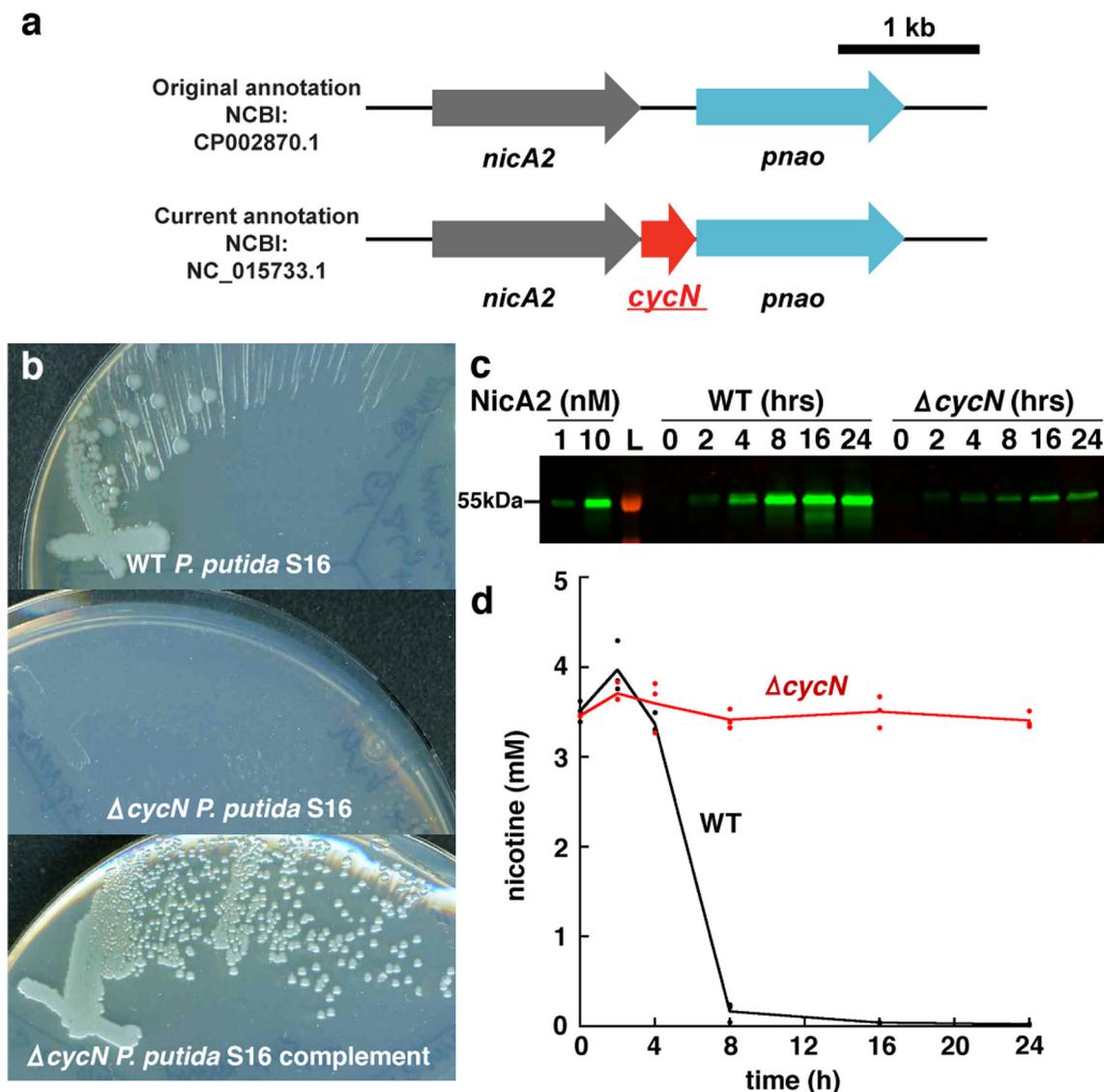
Figure 2 |. A *cycN* knockout is unable to grow on or degrade nicotine.
a, Top: The gene annotations when the genome of *P. putida* S16 was originally sequenced[21]. Bottom: The updated gene annotations currently available from NCBI show an uncharacterized cytochrome c-encoding gene WP_080563818.1 between *nicA2* (PPS_RS28245) and *pnao* (PPS_RS21095), which we termed *cycN* (PPS_RS28240). **b**, Single colonies of *P. putida* S16 were streaked onto M9 salts agar supplemented with nicotine and imaged after two days of growth at 30 °C. The WT strain showed robust growth, whereas the *cycN* strain grew poorly. Plasmid-based expression of *cycN* complemented the knockout. **c**, Quantitative western blots against NicA2 (green) in *P. putida* S16 lysates show expression of NicA2 as induced by nicotine in both the WT and *cycN* strains over time. Purified NicA2 of known concentration was included as a loading control. **d**, Nicotine concentration as determined from cell culture by HPLC demonstrates decreasing concentration of nicotine over time in the WT strain, with no decrease in a *cycN* strain. These experiments were independently repeated twice with similar results.
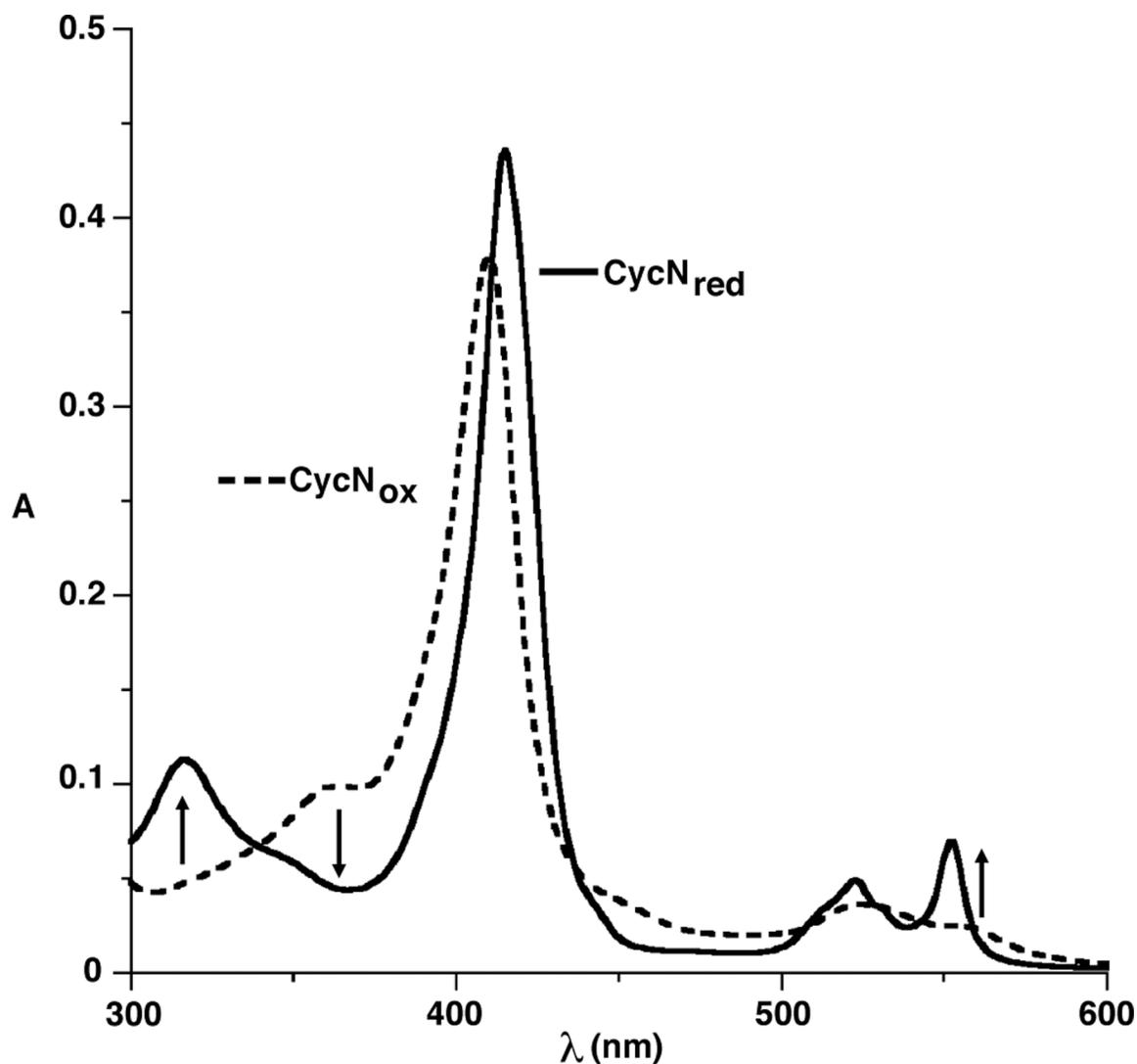
Figure 3 |. CycN is reduced by NicA2.
Oxidized CycN (dashed line) under ambient conditions was monitored by UV-vis
spectrophotometry. Upon addition of 30 nM NicA2 and 100 µM nicotine, 3.75 µM CycN
showed an increase in absorbance typical for reduced cytochrome c at 410 and 550 nm
(solid line), indicating that CycN had become reduced. Arrows indicate the directionality of
change. Both NicA2 and nicotine are required to produce this change, as adding either one
individually failed to reduce CycN. This experiment was independently repeated twice with
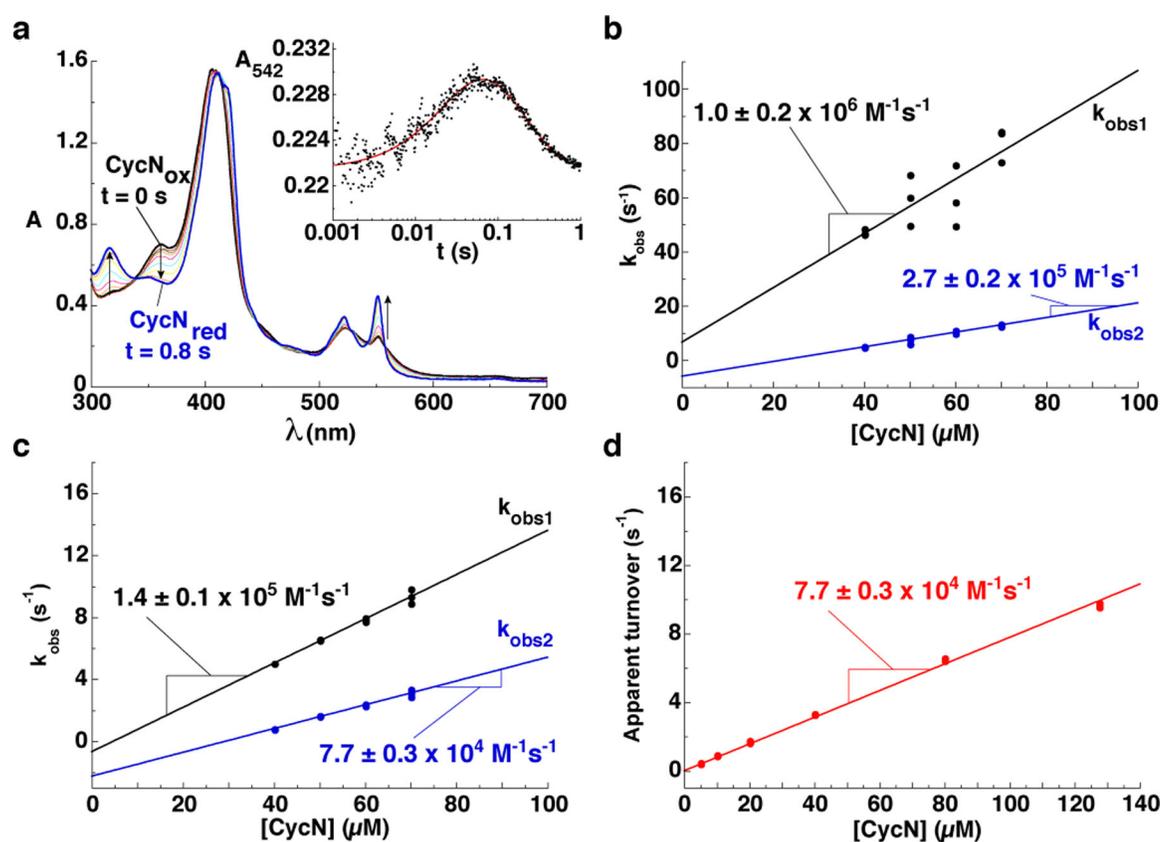similar results.

Figure 4 |. NicA2 is rapidly oxidized by CycN.

a, Oxidized CycN and reduced NicA2 were mixed in a series of anaerobic stopped-flow spectrophotometry experiments. Upon mixing, the absorbance changes were dominated by CycN reduction. Inset: The signal was monitored at 542 nm (an isosbestic point for CycN reduction/oxidation) in order to observe spectral changes only associated with NicA2 FAD absorbance. Note the logarithmic timescale. Traces at this wavelength fit well to two exponentials. See Extended Data Figure 9a for kinetic traces at all CycN concentrations. **b**, k_{obs} values determined for the first phase were plotted against the concentration of CycN in each experiment, demonstrating linear dependence. The y-intercept was 6 ± 12 s^{-1}. The k_{obs} values for the second phase were also linearly dependent with CycN concentration. The negative y-intercept for k_{obs2} (-5.9 ± 1.0 s^{-1}) is likely a result of the CycN concentration for the second phase being lower than the initial CycN concentration since roughly one NicA2 equivalent worth of CycN is consumed in the first phase. **c,** the k_{obs} values obtained for the reaction of oxidized CycN with N-methylmyosmine-bound NicA2 containing reduced FAD. The k_{obs} values for both phases increased linearly with CycN concentration. The y-intercepts for k_{obs1} and k_{obs2} were -0.6 ± 0.3 s^{-1} and -2.2 ± 0.2 s^{-1}, respectively. The large negative y-intercept for k_{obs2} was again likely due to the consumption of some CycN in the first phase. **d,** The apparent steady state turnover number for NicA2 using saturating nicotine (1 mM) and varying amounts of CycN. When fit by a line, the slope of the steady state data matched that of the second NicA2–CycN oxidation event for N-methylmyosmine-bound NicA2. Values reported are the mean ± s.e.m. of the fit for all panels. These experiments were independently repeated twice with similar results.
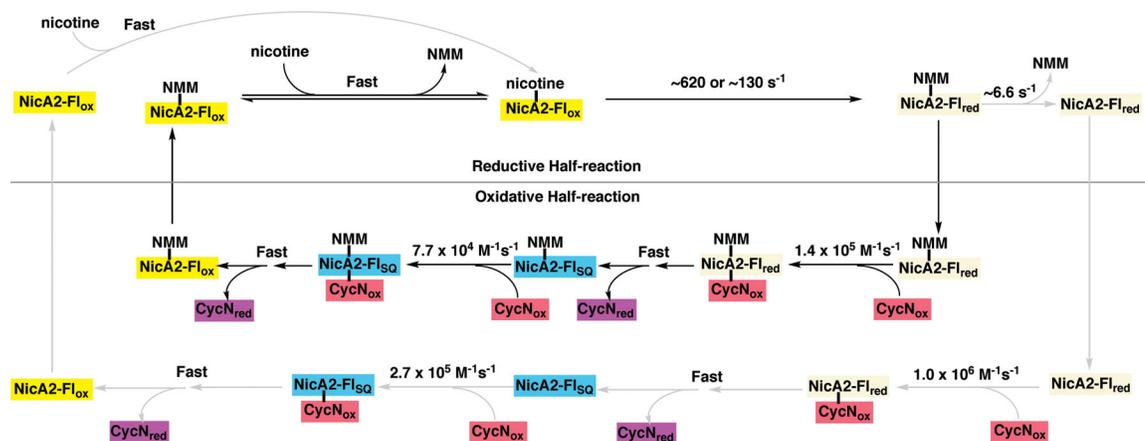
Figure 5 |. Proposed kinetic mechanism for the catalytic cycle of NicA2.
N-methylmyosmine (NMM) is the product resulting from the NicA2-catalyzed oxidation of nicotine. NicA2-Fl$_{ox}$, NicA2 containing oxidized FAD; NicA2-Fl$_{red}$, NicA2 containing FADH$_2$; NicA2-Fl$_{SQ}$, NicA2 containing a flavin semiquinone. Only the black path is relevant during catalytic turnover by the enzyme.